



# Synthesis, properties, and reactivity of a series of non-heme {FeNO}<sup>7/8</sup> complexes: Implications for Fe-nitroxyl coordination

Brian C. Sanders, Ashis K. Patra, Todd C. Harrop\*

Department of Chemistry, The University of Georgia, 1001 Cedar Street, Athens, GA 30602, USA  
Center for Metalloenzyme Studies, The University of Georgia, 1001 Cedar Street, Athens, GA 30602, USA

## ARTICLE INFO

### Article history:

Received 12 June 2012

Received in revised form 17 August 2012

Accepted 18 August 2012

Available online 6 October 2012

## ABSTRACT

The biochemical properties of nitroxyl (HNO/NO<sup>-</sup>) are distinct from nitric oxide (NO). Metal centers, particularly Fe, appear as suitable sites of HNO activity, both for generation and targeting. Furthermore, reduced Fe–NO<sup>-</sup>/Fe–HNO or {FeNO}<sup>8</sup> (Enemark–Feltham notation) species offer unique bonding profiles that are of fundamental importance. Given the unique chemical properties of {FeNO}<sup>8</sup> systems, we describe herein the synthesis and properties of {FeNO}<sup>7</sup> and {FeNO}<sup>8</sup> non-heme complexes containing pyrrole donors that display heme-like properties, namely [Fe(LN<sub>4</sub><sup>R</sup>)(NO)] (R = C<sub>6</sub>H<sub>4</sub> or Ph for **3**; and R = 4,5-Cl<sub>2</sub>C<sub>6</sub>H<sub>2</sub> or PhCl for **4**) and K[Fe(LN<sub>4</sub><sup>R</sup>)(NO)] (R = Ph for **5**; R = PhCl for **6**). X-ray crystallography establishes that the Fe–N–O angle is ~155° for **3**, which is atypical for low-spin square-pyramidal {FeNO}<sup>7</sup> species. Both **3** and **4** display  $\nu_{\text{NO}}$  at ~1700 cm<sup>-1</sup> in the IR and reversible diffusion-controlled cyclic voltammograms (CVs) (E<sub>1/2</sub> = ~-1.20 V vs. Fc/Fc<sup>+</sup> (ferrocene/ferrocenium redox couple) in MeCN) suggesting that the {FeNO}<sup>8</sup> compounds **5** and **6** are stable on the CV timescale. Reduction of **3** and **4** with stoichiometric KC<sub>8</sub> provided the {FeNO}<sup>8</sup> compounds **5** and **6** in near quantitative yield, which were characterized by the shift in  $\nu_{\text{NO}}$  to 1667 and ~1580 cm<sup>-1</sup>, respectively. While the  $\nu_{\text{NO}}$  for **6** is consistent with FeNO reduction, the  $\nu_{\text{NO}}$  for **5** appears more indicative of ligand-based reduction. Additionally, **5** and **6** engage in HNO-like chemistry in their reactions with ferric porphyrins [Fe<sup>III</sup>(TPP)X] (TPP = tetraphenylporphyrin; X = Cl<sup>-</sup>, OTf<sup>-</sup> (trifluoromethanesulfonate anion or CF<sub>3</sub>SO<sub>3</sub><sup>-</sup>)) to form [Fe(TPP)NO] in stoichiometric yield via reductive nitrosylation.

© 2012 Elsevier Inc. All rights reserved.

## 1. Introduction

The one-electron reduced analogue of nitric oxide (NO•), termed a nitroxyl or nitrosyl hydride (HNO or NO<sup>-</sup> (nitroxyl anion) depending on the pH; pK<sub>a</sub> = 11.6) [1,2], has received special attention of late including this thematic issue of the *Journal of Inorganic Biochemistry*. Most research on this enigmatic inorganic small molecule stems from its potential as a therapeutic [3]. For example, HNO has been shown to increase myocardial contractility, i.e. the strength of heart muscle tissue, and thus represents a promising drug for heart failure [4–6]. In fact, HNO is already clinically approved for other disease treatments. This includes the HNO-donor molecule cyanamide (N-hydroxycyanamide is the actual HNO-donor), which has shown to be an effective anti-alcoholism drug by disturbing alcohol metabolism through inhibiting the enzyme aldehyde dehydrogenase [7,8]. The mechanism of action of HNO appears to be through its interactions with thiol-containing biomolecules [9–11] and ferric heme proteins [1,12–16]. While the endogenous production of HNO has not been clearly established, there is evidence of its formation from

nitric oxide synthase (NOS) in the absence of its biopterin cofactor [17]. Additionally, iron-coordinated HNO/NO<sup>-</sup> are proposed intermediates of the enzymes involved in denitrification, namely nitrite reductase (NiR) and nitric oxide reductase (NOR) [12,18–21]. However, the basic chemistry and biology of this small molecule are challenging to study. The short half-life of HNO, due to the self-condensation reaction to form nitrous oxide (N<sub>2</sub>O) and water, necessitates the use of *reliable* HNO-donor molecules to understand its fundamental biochemical reactions [1,3,14,17,22,23]. The most commonly employed HNO-donors are Angeli's salt (Na<sub>2</sub>N<sub>2</sub>O<sub>3</sub>) [24,25], derivatives of Piloty's acid (sulfohydroxamic acids) [3,26], and others [27,28] making this quite an active area of research in the HNO field. As such, there still remains much to be answered in terms of the chemistry and biology of HNO.

First-row transition metals, especially iron, appear to be among the most likely sites for the potential endogenous generation and targets of HNO [1,3,12,15,17,18,29]. Metal–NO complexes are typically defined by the notation of Enemark and Feltham (EF notation) that describes the total number of electrons in this delocalized bond as a post-superscript, designated as {MNO}<sup>n</sup> [30]. Iron nitroxyl complexes proposed to form in denitrifying enzymes are thus classified as {FeNO}<sup>8</sup> or {FeHNO}<sup>8</sup> depending on the pH. Despite their importance

\* Corresponding author. Tel.: +1 706 542 3486; fax: +1 706 542 9454.  
E-mail address: [tharrop@uga.edu](mailto:tharrop@uga.edu) (T.C. Harrop).

in defining the fundamental coordination chemistry of HNO with Fe in biology, there remains a paucity of information on this class of iron-nitrosyls.

The pioneering work by Kadish and Ryan on the  $\{\text{FeNO}\}^8$  complexes of tetraphenylporphyrin (TPP) and octaethylporphyrin (OEP) represents the first foray into this unique EF notation (see Chart 1, Table 1) [31–33]. Both  $[\text{Fe}(\text{TPP})\text{NO}]^-$  and  $[\text{Fe}(\text{OEP})\text{NO}]^-$  were studied in situ by spectroelectrochemistry where they displayed reversible  $\{\text{FeNO}\}^7/\{\text{FeNO}\}^8$  redox couples at relatively low potentials ( $\sim -1$  V vs. SCE = saturated calomel reference electrode) in a variety of solvents (Table 1) [31–33]. While these derivatives were never isolated as discrete solids (even after exhaustive electrolysis), vibrational data (Table 1) was obtained on these systems, which exhibited NO stretching frequencies ( $\nu_{\text{NO}}$ ) at  $\sim 1500$   $\text{cm}^{-1}$  [31]. The first and only isolated heme  $\{\text{FeNO}\}^8$  analogue,  $[\text{Co}(\text{Cp})_2][\text{Fe}(\text{TFPPBr}_8)(\text{NO})]$  (Chart 1; where  $\text{TFPPBr}_8$  is the dianion of 2,3,7,8,12,13,17,18-octabromo-5,10,15,20-[tetrakis-(pentafluorophenyl)]porphyrin), was reported just recently in 2010 by Doctorovich and coworkers [34,35]. Extensive halogenation of the TPP framework resulted in a significant stabilization of this  $\{\text{FeNO}\}^8$  derivative and is represented by the cathodic shift in  $E_{1/2}$  to  $-0.20$  V (vs. SCE in  $\text{CH}_2\text{Cl}_2$ ) and corresponding blue-shift in  $\nu_{\text{NO}}$  to  $\sim 1550$   $\text{cm}^{-1}$  from the TPP derivative [34]. Additional theoretical work by Lehnert and Rodgers has also helped establish the structural and spectroscopic features of heme  $\{\text{Fe}(\text{H})\text{NO}\}^8$  complexes although no small molecule has been characterized by any structural methods [36,37]. Farmer's group, however, was successful in obtaining structural information on the  $\{\text{FeHNO}\}^8$  complex with myoglobin, which is apparently very stable [38–40]. The X-ray absorption experiments revealed Fe–N and N–O lengths of 1.82 and 1.24 Å, respectively, with a severely bent Fe–N–O angle of  $131^\circ$  [38]. These values were largely in agreement with theoretical calculations for small molecules with diamagnetic ground states. Non-heme examples of  $\{\text{FeNO}\}^8$  are even rarer with a total of three such reported complexes [41,42] to date and only one being isolable [43]. The extensive spectroscopic studies by Wieghardt on  $[\text{Fe}(\text{cyclam-ac})(\text{NO})]$  represent the first reported non-heme derivative [42]. While these studies were performed on in situ generated material at low temperature, they were the first to include Mössbauer studies on an  $\{\text{FeNO}\}^8$  complex ( $\delta$ : 0.41 mm/s,  $\Delta E_Q$ : 1.69 mm/s) and report the lowest  $\nu_{\text{NO}}$  ( $1271$   $\text{cm}^{-1}$ ) of all  $\{\text{FeNO}\}^8$  complexes [42]. These values were consistent with a low-spin (LS) Fe(II) ( $S=0$ ) coordinated to a singlet  $^1\text{NO}^-$  ( $S=0$ ) assignment.

**Table 1**  
Electrochemical and spectroscopic data of  $\{\text{FeNO}\}^8$  systems.

Complex	$E_{1/2}$ (V) <sup>a</sup>	$\nu_{\text{NO}}$ ( $\text{cm}^{-1}$ )	$\Delta\nu_{\text{NO}}$ ( $\text{cm}^{-1}$ ) <sup>b</sup>	Ref.
$[\text{Fe}(\text{LN}_4^{\text{ph}})(\text{NO})]^-$ (5)	$-0.83^c$	$\sim 1580^d$	$-140$	This work
$[\text{Fe}(\text{LN}_4^{\text{cl}})(\text{NO})]^-$ (6)	$-0.76^c$	$1667^d$	$-43$	This work
$[\text{Fe}(\text{LN}_4^{\text{f}})(\text{NO})]^-$ (7)	$-0.98^c$	$1604^d$	$-100$	[43]
$[\text{Fe}(\text{TPP})\text{NO}]^-$	$-0.93^c$	$1496^f$	$-185$	[31,33]
$[\text{Fe}(\text{OEP})\text{NO}]^-$	$-1.08^g$	$1441^f$	$-229$	[59]
$[\text{Fe}(\text{TFPPBr}_8)(\text{NO})]^-$	$-0.19^e$	$\sim 1550^d$	$-176$	[34]
<i>trans</i> - $[\text{Fe}(\text{NO})(\text{cyclam-ac})]$	$-0.99^c$	$1271^c$	$-336$	[42]
$[\text{Fe}(\text{CN})_5(\text{HNO})]^{3-}$	$-1.00^h$	$1384^h$	$-264$	[41]

<sup>a</sup> Data represents the  $E_{1/2}$  value for the  $\{\text{FeNO}\}^7/\{\text{FeNO}\}^8$  redox couple employing the isolated  $\{\text{FeNO}\}^7$  complexes and normalized to the saturated calomel reference electrode (SCE) based on information found in Geiger [60].

<sup>b</sup> Denotes the change in N–O stretching frequency upon reduction from  $\{\text{FeNO}\}^7$  to  $\{\text{FeNO}\}^8$ .

<sup>c</sup> MeCN.

<sup>d</sup> KBr.

<sup>e</sup>  $\text{CH}_2\text{Cl}_2$ .

<sup>f</sup> THF- $d_8$ .

<sup>g</sup> THF.

<sup>h</sup>  $\text{H}_2\text{O}$ .

The IR value is in-line with another non-heme  $\{\text{FeHNO}\}^8$  complex,  $[\text{Fe}(\text{CN})_5(\text{HNO})]^{3-}$  (Chart 1), which displays a  $\nu_{\text{NO}}$  of  $1380$   $\text{cm}^{-1}$  [41]. The only non-heme protein  $\{\text{FeNO}\}^8$  example has been produced by cryoreduction of the  $\{\text{FeNO}\}^7$  adduct of the taurine: $\alpha$ -ketoglutarate dioxygenase (TauD) enzyme [44]. This study was the first and is still the only to report a paramagnetic  $\{\text{FeNO}\}^8$  species from an extensive theoretical calibration of valid bonding models with experimental Mössbauer parameters ( $\delta$ : 1.07 mm/s,  $\Delta E_Q$ : 2.39 mm/s). These results contrast those obtained for  $[\text{Fe}(\text{cyclam-ac})(\text{NO})]$  due to the triplet ground state of  $\text{TauD-}\{\text{FeNO}\}^8$  that has been assigned as a high-spin (HS) Fe(II) ( $S=2$ ) antiferromagnetically coupled to triplet  $^3\text{NO}^-$  ( $S=1$ ). This small collection of reported  $\{\text{Fe}(\text{H})\text{NO}\}^8$  complexes has led to some general properties of  $\{\text{FeNO}\}^8$ : (i) the preference of  $S=0$  (diamagnetic) ground states (TauD being the only outlier) suggestive of a coordinated singlet nitroxyl or nitroxyl anion ( $^1\text{HNO}$  or  $^1\text{NO}^-$ ); (ii)  $\nu_{\text{NO}}$  values of  $\sim 1500$   $\text{cm}^{-1}$  for heme;  $\sim 1300$   $\text{cm}^{-1}$  for non-heme with the exception of MbHNO ( $\nu_{\text{NO}}$ :  $1385$   $\text{cm}^{-1}$ ) [38,45]; and (iii) low  $E_{1/2}$  values for the  $\{\text{FeNO}\}^7/\{\text{FeNO}\}^8$  redox couple of  $\sim -1$  V (vs. SCE) with one noted exception in  $[\text{Fe}(\text{TFPPBr}_8)(\text{NO})]$ . Although several theoretical and spectroscopic

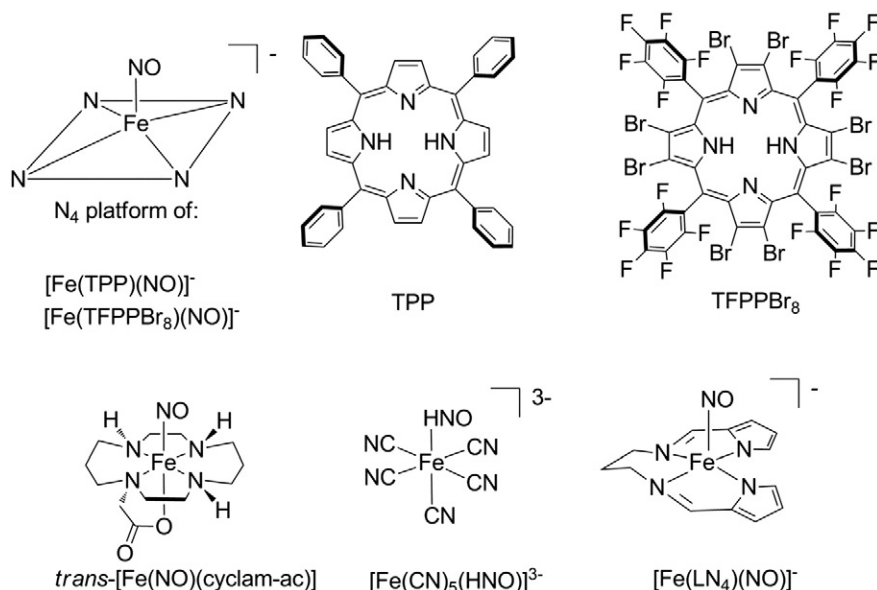


**Chart 1.** Representative structures of reported low molecular weight  $\{\text{Fe}(\text{H})\text{NO}\}^8$  coordination complexes.

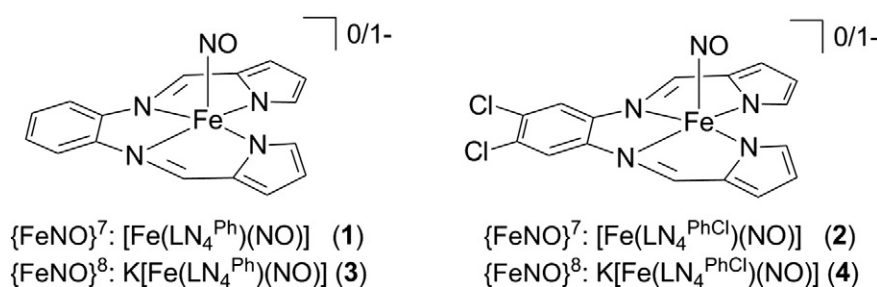


Chart 2. Iron nitrosyl complexes reported in this work.

examinations have shed some insight on the elusive  $\{\text{FeNO}\}^8$  species, the reactivity of these systems has not been thoroughly explored.

As part of our continuing efforts to establish the defining features of this unique class of iron–nitrosyls and a means of understanding biological Fe–nitrosyl interactions, we describe herein the synthesis and properties of several iron coordination complexes utilizing a heme-like diimine/dipyrroloide  $\text{N}_4$  supporting ligand, namely  $(\text{Et}_4\text{N})[\text{Fe}(\text{LN}_4^{\text{Ph}})\text{Cl}]$  (1),  $(\text{Et}_4\text{N})[\text{Fe}(\text{LN}_4^{\text{PhCl}})\text{Cl}]$  (2),  $[\text{Fe}(\text{LN}_4^{\text{Ph}})(\text{NO})]$  (3),  $[\text{Fe}(\text{LN}_4^{\text{PhCl}})(\text{NO})]$  (4),  $\text{K}[\text{Fe}(\text{LN}_4^{\text{Ph}})(\text{NO})]$  (5), and  $\text{K}[\text{Fe}(\text{LN}_4^{\text{PhCl}})(\text{NO})]$  (6) (see Chart 2 for  $\{\text{FeNO}\}^{7/8}$  complexes 3–6). We previously published a detailed account of the synthesis and properties of the first isolable non-heme  $\{\text{FeNO}\}^8$  complex,  $[\text{Co}(\text{Cp}^*)_2][\text{Fe}(\text{LN}_4^{\text{PT}})(\text{NO})]$ , where we established its nitroxyl-like reactivity with met-myoglobin under pseudo-physiological conditions [43]. Seeking to add to the list of isolable  $\{\text{FeNO}\}^8$  complexes, we describe in this paper new  $\{\text{FeNO}\}^8$  complexes based on similar ligand backbones with subtle electronic/structural differences as a logical extension of our previous study. The objective of the present contribution was to define new synthetic strategies to access Fe–nitrosyls and to understand the fundamental spectroscopic, structural, and reaction chemistry of isolable  $\{\text{FeNO}\}^8$  systems. The long-term goal is to utilize this knowledge in (i) establishing spectroscopic benchmarks for Fe–(H)NO intermediates traversed in biological denitrification and (ii) the development of metal-based HNO donors with therapeutic applications.

## 2. Materials and methods

### 2.1. General information

All reagents were procured from commercial suppliers and used as received unless otherwise noted. Research grade nitric oxide gas,  $\text{NO}(\text{g})$ , UHP, 99.5% was obtained from Matheson Tri-Gas. The  $\text{NO}(\text{g})$  was purified by passage through an Ascarite II® column (sodium hydroxide-coated silica, purchased from Aldrich) and handled under anaerobic conditions.  $^{15}\text{NO}(\text{g})$  ( $^{15}\text{N}$ ,  $\geq 98\%$ ) was purchased from Cambridge Isotope Laboratories and used without further purification. Acetonitrile (MeCN), methylene chloride ( $\text{CH}_2\text{Cl}_2$ ), tetrahydrofuran (THF), diethyl ether ( $\text{Et}_2\text{O}$ ) and pentane were purified by passage through activated alumina columns using an MBraun MB-SPS solvent purification system and stored over 3 Å molecular sieves under a nitrogen ( $\text{N}_2$ ) atmosphere before use. *N,N*-dimethylformamide (DMF) was purified with a VAC solvent purifier containing 4 Å molecular sieves and was stored under similar conditions. Anhydrous MeOH and EtOH were obtained by distilling the alcohol from  $\text{Mg}(\text{OR})_2$  ( $\text{R} = \text{Me}$  for MeOH, Et for EtOH) and stored under  $\text{N}_2$ . Toluene was purified by stirring overnight with 3 Å molecular sieves, then distilling from  $\text{CaH}_2$ , which was finally stored over 3 Å molecular sieves. Acetone was dried by stirring over 3 Å molecular sieves for 24 h, which was decanted and stored under  $\text{N}_2$ . All solvents were filtered to remove sieve particulate with a 0.45  $\mu\text{m}$  nylon filter immediately before use. The Fe(II) salt,  $(\text{Et}_4\text{N})_2[\text{FeCl}_4]$  [46], and  $\{\text{FeNO}\}^7$  complex,  $[\text{Fe}(\text{TPP})\text{NO}]$  [47], were prepared according to the published procedures. All reactions were performed

under an inert atmosphere of  $\text{N}_2$  using standard Schlenk-line techniques or in an MBraun Labmaster glovebox under an atmosphere of purified  $\text{N}_2$ . All reactions and measurements involving  $\text{NO}(\text{g})$  and the FeNO complexes were performed in the dark with minimal light exposure by wrapping the reaction flasks/vials with aluminum foil to avoid any photochemical reactions.

### 2.2. Physical methods

FTIR spectra were collected with a Thermo Nicolet 6700 spectrophotometer running the OMNIC software. Samples were run as solids as KBr pellets in a stream of dry  $\text{N}_2$ . Solution FTIR spectra were obtained using a demountable airtight liquid IR cell from Graseby-Specac with  $\text{CaF}_2$  windows and 0.1 mm spacers. All FTIR samples were prepared inside a glovebox. The closed liquid cell was taken out of the box and spectra were acquired immediately. Room temperature (RT) solid-state magnetic susceptibility measurements were performed with a Johnson Matthey magnetic susceptibility balance. Solution-state susceptibility measurements were performed in a solution at 298 K using the Evans method on a Varian Unity Inova 500 MHz NMR spectrometer [48]. X-band (9.60 GHz) EPR spectra were obtained on a Bruker ESP 300E EPR spectrometer controlled with a Bruker microwave bridge at 10 K. The EPR was equipped with a continuous-flow liquid He cryostat and a temperature controller (ESR 9) made by Oxford Instruments, Inc. Electronic absorption spectra were run at 298 K using a Cary-50 UV-visible (UV-vis) spectrophotometer containing a Quantum Northwest TC 125 temperature control unit. The UV-vis samples were prepared anaerobically in gas-tight Teflon-lined screw cap quartz cells with an optical pathlength of 1 cm. Electrochemistry measurements were performed with a PAR Model 273A potentiostat using a  $\text{Ag}/\text{Ag}^+$  (0.01 M  $\text{AgNO}_3$ /0.1 M  $^n\text{Bu}_4\text{NPF}_6$  in  $\text{CH}_3\text{CN}$ ) reference electrode, Pt-wire counter electrode, and a glassy carbon working milli-electrode (diameter = 2 mm) under an Ar atmosphere. Measurements were performed at ambient temperature using 1.0–10.0 mM analyte in various solvents containing 0.1 M  $^n\text{Bu}_4\text{NPF}_6$  as the supporting electrolyte. Ferrocene (Fc) was used as an internal standard and all potentials are reported relative to the  $\text{Fc}^+/\text{Fc}$  couple.  $^1\text{H}$  and  $^{13}\text{C}$  NMR spectra were recorded in the listed deuterated solvent on a 400 MHz Bruker BZH 400/52 NMR spectrometer or a Varian Unity Inova 500 MHz NMR at 298 K with chemical shifts referenced to TMS (tetramethylsilane =  $\text{Si}(\text{CH}_3)_4$ ) or residual protio signal of the deuterated solvent as previously reported [49]. Low resolution ESI-MS (electrospray ionization mass spectrometry) data were collected on a Perkin Elmer Sciex API I Plus quadrupole mass spectrometer whereas high resolution ESI-MS data were collected using a Bruker Daltonics 9.4 T APEXQh FT-ICRM. Elemental microanalyses for C, H, and N were performed by QTI-Intertek (Whitehouse, NJ) or Columbia Analytical Services (Tucson, AZ). For some complexes, notably 5–6, residual solvent is present in the microanalysis and is consistent with what is observed for these compounds in their solid-state IR spectra.

### 2.3. Synthesis of compounds

#### 2.3.1. Synthesis of (N1E,N2E)-N1,N2-bis((1H-pyrrol-2-yl)methylene)-benzene-1,2-diamine (LN<sub>4</sub>H<sub>2</sub><sup>Ph</sup>)

To an anaerobic solution of 1,2-phenylenediamine (2.161 g, 19.98 mmol) in 25 mL of MeCN was added a 25 mL MeCN solution containing 3.801 g (39.97 mmol) of pyrrole-2-carboxaldehyde followed by addition of activated 3 Å molecular sieves (15% w/v). The brown solution mixture was refluxed for 24 h and allowed to cool to RT before workup. Once cooled the red mixture was filtered (sieves and insoluble yellow product) and the insolubles were washed with CHCl<sub>3</sub>. The red filtrate was concentrated under vacuum to afford a red amorphous paste that was dried for several hours under reduced pressure prior to trituration with ~30 mL of Et<sub>2</sub>O. The insoluble yellow material was filtered, washed with cold Et<sub>2</sub>O, and dried under vacuum to afford 3.255 g (12.36 mmol, 62%) of product. Mp: 197–199 °C. <sup>1</sup>H NMR (400 MHz, CDCl<sub>3</sub>, δ from TMS): 12.34 (br, 1H, NH), 7.68 (s, 1H, CH=N), 7.25 (t, 1H, Ar-H), 7.07 (dd, 1H, Ar-H), 6.40 (d, 1H, Ar-H pyrrole), 6.23 (s, 1H, Ar-H pyrrole), and 6.01 (t, 1H, Ar-H pyrrole). <sup>13</sup>C NMR (100.6 MHz, CDCl<sub>3</sub>): 150.7 (CH=N), 145.9 (Ar-C), 131.0 (Ar-C), 126.8 (Ar-C), 123.9 (Ar-C), 119.1 (Ar-C), 117.3 (Ar-C), and 109.7 (Ar-C). FTIR (KBr matrix), ν<sub>max</sub> (cm<sup>-1</sup>): 3445 (w), 3141 (m), 3085 (w), 2970 (w), 2855 (w), 2746 (w), 1617 (vs), 1574 (s), 1549 (m), 1485 (w), 1442 (m), 1412 (s), 1336 (m), 1310 (m), 1275 (w), 1247 (w), 1211 (m), 1189 (w), 1160 (w), 1138 (m), 1094 (s), 1036 (s), 1026 (s), 971 (w), 966 (w), 884 (m), 877 (m), 846 (m), 801 (w), 783 (w), 742 (s), 659 (w), 608 (m), 579 (w), and 551 (m). LRMS-ESI (*m/z*): [M + H]<sup>+</sup> calcd for C<sub>16</sub>H<sub>15</sub>N<sub>4</sub>, 263.1; found, 263.2.

#### 2.3.2. Synthesis of (N1E,N2E)-N1,N2-bis((1H-pyrrol-2-yl)methylene)-4,5-dichlorobenzene-1,2-diamine (LN<sub>4</sub>H<sub>2</sub><sup>PhCl</sup>)

Under anaerobic conditions, a 5 mL MeCN solution of 1.004 g (5.671 mmol) of 4,5-dichlorobenzene-1,2-diamine was added to a 5 mL MeCN solution containing 1.074 g (11.29 mmol) of pyrrole-2-carboxaldehyde in the presence of 3 Å molecular sieves (15% w/v). This solution was then refluxed overnight at 70 °C for 20 h resulting in a black-to-deep-red color change over the reflux period. Cooling the resulting mixture to RT resulted in the precipitation of a dark insoluble material. The insolubles (product and sieves) were filtered through a glass frit, thoroughly washed with CHCl<sub>3</sub>, and the filtrate was concentrated and dried in vacuo to a dark red paste. The material was then redissolved in minimal MeCN (~10 mL) and kept at -5 °C to induce precipitation of the desired product. The procedure of concentration, dissolution in minimal MeCN, and precipitation was repeated three times to afford the dark red-brown solid product (1.110 g, 3.341 mmol, 59%). Mp: 191–194 °C. <sup>1</sup>H NMR (400 MHz, CDCl<sub>3</sub>, δ from residual protio solvent): 11.87 (br, 0.7H, NH, integrates slightly low due to the exchangeable nature of the pyrrole proton), 7.64 (s, 1H, CH=N), 7.16 (s, 1H, Ar-H), 6.48 (d, 1H, Ar-H pyrrole), 6.38 (d, 1H, Ar-H pyrrole), 6.10 (t, 2H, Ar-H pyrrole). <sup>13</sup>C NMR (100.6 MHz, CDCl<sub>3</sub>): 151.5 (CH=N), 145.3 (Ar-C), 130.6 (Ar-C), 129.6 (Ar-C), 124.5 (Ar-C), 120.7 (Ar-C), 118.8 (Ar-C) and 110.6 (Ar-C). FTIR (KBr matrix), ν<sub>max</sub> (cm<sup>-1</sup>): 3446 (w), 3140 (w), 2967 (w), 2890 (w), 2847 (w), 2745 (w), 1611 (vs), 1567 (m), 1484 (w), 1471 (w), 1435 (w), 1413 (s), 1374 (w), 1355 (m), 1331 (m), 1312 (m), 1263 (w), 1245 (w), 1223 (w), 1163 (m), 1126 (s), 1092 (m), 1032 (s), 961 (w), 887 (m), 856 (w), 831 (w), 808 (w), 741 (m), 678 (w), 652 (w), 605 (m), 594 (m), 505 (w), 497 (w), 440 (w), and 429 (w). LRMS-ESI (*m/z*): [M + H]<sup>+</sup> calcd for C<sub>16</sub>H<sub>13</sub>Cl<sub>2</sub>N<sub>4</sub>, 331.1; found, 331.2.

#### 2.3.3. Synthesis of (Et<sub>4</sub>N)[Fe(LN<sub>4</sub><sup>Ph</sup>)Cl] (1)

To a batch of LN<sub>4</sub>H<sub>2</sub><sup>Ph</sup> (0.2500 g, 0.9531 mmol) dispersed in 5 mL of dry MeCN was added a 3 mL MeCN slurry of NaH (0.0457 g, 1.904 mmol), resulting in H<sub>2</sub>(g) evolution and a color change from orange-yellow to bright yellow indicative of ligand deprotonation.

To ensure complete deprotonation, an occasional vacuum was applied while stirring for ~15 min. To this reaction mixture was then added a 10 mL MeCN solution of (Et<sub>4</sub>N)<sub>2</sub>[FeCl<sub>4</sub>] (0.4366 g, 0.9529 mmol) resulting in the formation of a pale gray-white precipitate (NaCl) and a solution color change to dark brown-yellow. The reaction mixture was stirred for another 2 h at RT, which resulted in no further change. The solution was filtered of insolubles and the homogeneous dark filtrate was stripped of MeCN and treated with ~20 mL of THF to precipitate any excess Et<sub>4</sub>NCl. The THF insolubles were filtered and washed with THF, and the dark filtrate was concentrated and dried under vacuum resulting in **1** as a shiny dark solid (0.3582 g, 0.7434 mmol, 78%). FTIR (KBr matrix), ν<sub>max</sub> (cm<sup>-1</sup>): 3062 (w), 2975 (w), 2945 (w), 1589 (vs), 1557 (vs), 1481 (w), 1462 (m), 1437 (m), 1383 (s), 1288 (s), 1219 (m), 1183 (m), 1169 (m), 1100 (w), 1077 (w), 1027 (vs), 969 (m), 891 (m), 870 (m), 787 (m), 743 (s), 684 (w), 608 (m), 591 (m), 578 (m), 551 (w), 531 (w), and 480 (w). UV-vis (THF, 298 K), λ<sub>max</sub>, nm (ε, M<sup>-1</sup> cm<sup>-1</sup>): 313 (12,900), 364 (27,000), and 414 (16,200). Anal. calcd for C<sub>24</sub>H<sub>32</sub>N<sub>5</sub>ClFe·0.5 H<sub>2</sub>O: C, 58.73; H, 6.78; N, 14.27. Found: C, 58.76; H, 6.44; N, 13.92.

#### 2.3.4. Synthesis of (Et<sub>4</sub>N)[Fe(LN<sub>4</sub><sup>PhCl</sup>)Cl] (2)

To a batch of LN<sub>4</sub>H<sub>2</sub><sup>PhCl</sup> (0.3001 g, 0.9061 mmol) dispersed in 8 mL of MeCN was added a 3 mL MeCN slurry of NaH (0.0435 g, 1.813 mmol), which resulted in H<sub>2</sub>(g) evolution and a dark brown-green solution indicative of ligand deprotonation. To ensure complete deprotonation, an occasional vacuum was applied while stirring the solution for ~15 min. To this solution was then added a 5 mL MeCN slurry of (Et<sub>4</sub>N)<sub>2</sub>[FeCl<sub>4</sub>] (0.4151 g, 0.9060 mmol) resulting in the formation of a pale gray-white precipitate (NaCl) and a solution color change to dark brown-yellow. The reaction mixture was stirred for another 2 h at RT, which resulted in no further change. The solution was then filtered to obtain a homogeneous dark filtrate. The filtrate was stripped to dryness, and treated with 20 mL of THF to precipitate any free Et<sub>4</sub>NCl. The THF insolubles were filtered and washed with THF, and the dark filtrate was concentrated and dried under vacuum resulting in a shiny dark black solid (0.4500 g, 0.8171 mmol, 90%). FTIR (KBr matrix), ν<sub>max</sub> (cm<sup>-1</sup>): 3080 (w), 2975 (w), 2945 (w), 1578 (vs), 1541 (vs), 1481 (w), 1457 (m), 1444 (m), 1434 (m), 1383 (s), 1292 (s), 1280 (s), 1254 (s), 1184 (m), 1170 (m), 1119 (m), 1076 (w), 1029 (s), 998 (m), 970 (m), 891 (m), 867 (m), 809 (w), 784 (w), 758 (m), 745 (s), 683 (w), 672 (w), 609 (m), 538 (w), 493 (w), and 447 (m). UV-vis (THF, 298 K), λ<sub>max</sub>, nm (ε, M<sup>-1</sup> cm<sup>-1</sup>): 324 sh (14,000), 370 (33,000), and 430 (23,000). Anal. calcd. for C<sub>24</sub>H<sub>30</sub>Cl<sub>3</sub>FeN<sub>5</sub>·0.75 H<sub>2</sub>O: C, 51.09; H, 5.63; N, 12.41. Found: C, 51.19; H, 5.72; N, 12.10.

#### 2.3.5. Synthesis of [Fe(LN<sub>4</sub><sup>Ph</sup>)(NO)], {FeNO}<sup>7</sup> (3)

To an 8 mL MeCN solution of **1** (0.5951 g, 1.235 mmol) was purged NO(g) for 2 min at RT. The resulting solution changed immediately from brown-yellow to red-brown with concomitant precipitation of a dark microcrystalline solid. The reaction mixture was then stirred for 30 min at RT under an atmosphere of NO. After this time, excess NO(g) was removed in vacuo and replaced with N<sub>2</sub> and this solution was then placed in a -20 °C refrigerator for 1 h to precipitate more material. The microcrystalline product was filtered, washed with 6 mL of cold MeCN, and dried under vacuum to yield 0.351 g (1.01 mmol, 82%) of product. X-ray quality red crystals were grown by slow diffusion of pentane into a toluene solution of the complex at -20 °C. FTIR (KBr matrix), ν<sub>max</sub> (cm<sup>-1</sup>): 3088 (w), 3059 (w), 2999 (w), 1698 (vs, ν<sub>NO</sub>), 1583 (m), 1549 (s), 1506 (m), 1460 (w), 1443 (w), 1379 (s), 1323 (m), 1290 (s), 1256 (m), 1193 (m), 1170 (w), 1153 (w), 1077 (w), 1034 (s), 984 (m), 929 (m), 893 (m), 847 (w), 819 (w), 780 (m), 743 (s), 678 (m), 636 (w), 623 (m), 602 (m), 548 (w), 477 (w), 434 (w), and 419 (w). FTIR (solution); ν<sub>NO</sub> (cm<sup>-1</sup>): 1705 (MeCN); 1716 (2-MeTHF); 1716 (toluene); 1716 (CH<sub>2</sub>Cl<sub>2</sub>); μ<sub>eff</sub> (solution, 298 K): 2.4 BM in DMSO-*d*<sub>6</sub>. UV-vis (THF, 298 K), λ<sub>max</sub>, nm (ε, M<sup>-1</sup> cm<sup>-1</sup>): 309

sh (16,000), 359 (24,000), and 469 (10,000). Anal. calcd for  $C_{16}H_{12}FeN_5O$ : C, 55.52; H, 3.49; N, 20.23. Found: C, 55.27; H, 3.08; N, 20.24.

### 2.3.6. Synthesis of $[Fe(LN_4^{Ph})(^{15}NO)]$ , $\{Fe^{15}NO\}^7$ (**3-<sup>15</sup>NO**)

The isotopically-labeled complex was prepared in a similar procedure as **3** except for using  $^{15}NO(g)$  and 0.561 g (1.164 mmol) of **1**. Yield: 0.3550 g (1.025 mmol, 88%). FTIR,  $\nu_{NO}$  ( $cm^{-1}$ ): 1667 (KBr matrix,  $\Delta\nu_{NO}$  from natural abundant isotope in **3**: 31  $cm^{-1}$ ); 1680 (MeCN,  $\Delta\nu_{NO}$ : 25  $cm^{-1}$ ); 1681 (2-MeTHF,  $\Delta\nu_{NO}$ : 35  $cm^{-1}$ ); 1684 (toluene,  $\Delta\nu_{NO}$ : 32  $cm^{-1}$ ); 1685 ( $CH_2Cl_2$ ,  $\Delta\nu_{NO}$ : 31  $cm^{-1}$ ).

### 2.3.7. Synthesis of $[Fe(LN_4^{PhCl})NO]$ , $\{FeNO\}^7$ (**4**)

To a 10 mL MeCN solution containing 0.1401 g (0.2544 mmol) of **2** was purged a stream of purified  $NO(g)$  for 2 min at RT under dark conditions. Immediately upon introduction of  $NO(g)$ , a dark burgundy powdered solid appeared and the solution became red-burgundy in color. The reaction mixture was then stirred for 30 min at RT under an atmosphere of  $NO$  in the headspace of the flask. After this time, excess  $NO(g)$  was removed in vacuo and replaced with  $N_2$ . This solution was then placed in a  $-20^\circ C$  refrigerator for 1 h to precipitate more material. Finally, the powdered solid was filtered, washed with 3 mL of cold MeCN, and dried under vacuum to afford 0.0852 g (0.2048 mmol, 81%) of product. FTIR (KBr matrix),  $\nu_{max}$  ( $cm^{-1}$ ): 2922 (w), 1772 (w), 1720 (s,  $\nu_{NO}$ ), 1570 (s), 1542 (s), 1520 (s), 1500 (m), 1462 (w), 1449 (m), 1379 (s), 1327 (w), 1289 (m), 1272 (s), 1258 (m), 1193 (w), 1116 (w), 1039 (s), 982 (w), 924 (w), 912 (w), 881 (w), 854 (w), 810 (w), 752 (m), 679 (w), 653 (w), 600 (w), 549 (w), 522 (w), 470 (w), and 424 (w). FTIR (solution);  $\nu_{NO}$  ( $cm^{-1}$ ): 1722 ( $CH_2Cl_2$ ); 1716 (THF); 1702 (DMSO).  $\mu_{eff}$  (solution-state, 298 K): 2.1 BM in DMSO- $d_6$ . UV-vis (DMF, 298 K),  $\lambda_{max}$ , nm ( $\epsilon$ ,  $M^{-1} cm^{-1}$ ): 317 sh (22,000), 361 (31,000), and 478 sh (12,000); (THF, 298 K),  $\lambda_{max}$ , nm ( $\epsilon$ ,  $M^{-1} cm^{-1}$ ): 319 sh (14,000), 361 (21,000), and 480 (8600). Anal. calcd for  $C_{16}H_{10}Cl_2FeN_5O$ : C, 46.30; H, 2.43; N, 16.87. Found: C, 46.43; H, 2.57; N, 16.53.

### 2.3.8. Synthesis of $[Fe(LN_4^{PhCl})(^{15}NO)]$ , $\{Fe^{15}NO\}^7$ (**4-<sup>15</sup>NO**)

The isotopically-labeled complex **4-<sup>15</sup>NO** was prepared analogously to **4** except for using 0.1660 g (0.3014 mmol) of **4** dissolved in 5 mL of MeCN and  $^{15}NO(g)$ . Yield: 0.0951 g (0.2291 mmol, 76%). FTIR,  $\nu_{NO}$  ( $cm^{-1}$ ): 1686 (KBr matrix,  $\Delta\nu_{NO}$ : 34  $cm^{-1}$ ); 1684 (THF,  $\Delta\nu_{NO}$ : 32  $cm^{-1}$ ); 1663 (DMSO,  $\Delta\nu_{NO}$ : 39  $cm^{-1}$ ).

### 2.3.9. Synthesis of $K[Fe(LN_4^{Ph})(NO)]$ , $\{FeNO\}^8$ (**5**)

To a dark mixture of compound **3** (0.2000 g, 0.5778 mmol) in 5 mL of acetone was added  $KC_8$  (0.0850 g, 0.6288 mmol), which immediately formed a dark-red homogeneous solution (apart from the insoluble graphite). The mixture was allowed to stir for an additional 5 min prior to removal of the graphite by filtration. The filtrate was concentrated and treated with  $2 \times 5$  mL of  $Et_2O$ , which was decanted from the solid. The material was collected and dried to afford 0.2001 g (0.5194 mmol, 90%) of a dark-red solid product. FTIR (KBr matrix),  $\nu_{max}$  ( $cm^{-1}$ ): 3435 (w), 3069 (w), 2958 (w), 2917 (m), 2849 (m), 1705 (m,  $\nu_{CO}$ ), 1667 (m,  $\nu_{NO}$ ), 1589 (s), 1553 (s), 1463 (m), 1442 (w), 1382 (s), 1355 (m), 1285 (s), 1256 (m), 1223 (w), 1175 (w), 1092 (w), 1032 (s), 972 (w), 892 (w), 872 (w), 801 (w), 743 (s), 679 (w), 603 (w), 579 (w), 532 (w), and 481 (w). UV-vis (THF, 298 K),  $\lambda_{max}$ , nm ( $\epsilon$ ,  $M^{-1} cm^{-1}$ ): 364 (21,300), 409 (12,700), and 455 sh (8000). Anal. calcd for  $C_{16}H_{12}FeKN_5O \cdot acetone$ : C, 51.48; H, 4.09; N, 15.80. Found: C, 52.54; H, 3.75; N, 15.41. The compound may contain trace graphite ( $C_8$ ) from workup resulting in the higher than expected percent C.

### 2.3.10. Synthesis of $K[Fe(LN_4^{Ph})(^{15}NO)]$ , $\{Fe^{15}NO\}^8$ (**5-<sup>15</sup>NO**)

The isotopically-labeled complex **5-<sup>15</sup>NO** was prepared analogously to **5** except for using 0.0901 g (0.2603 mmol) of **3-<sup>15</sup>NO** dissolved in 3 mL of acetone and 0.0385 g (0.2848 mmol) of  $KC_8$ . Yield: 0.0871 g

(0.2261 mmol, 87%). FTIR,  $\nu_{NO}$  ( $cm^{-1}$ ): 1629 (KBr matrix,  $\Delta\nu_{NO}$ : 38  $cm^{-1}$ ).

### 2.3.11. Synthesis of $K[Fe(LN_4^{PhCl})(NO)]$ , $\{FeNO\}^8$ (**6**)

To a dark red heterogeneous mixture of **4** (0.1200 g, 0.2891 mmol) in 3 mL of acetone was added  $KC_8$  (0.0430 g, 0.3180 mmol), which immediately formed a homogeneous (apart from  $C_8$ ) darkened solution. This mixture was stirred for an additional 5 min at which point the insoluble  $C_8$  was removed by vacuum filtration and the acetone soluble filtrate was concentrated to dryness. The dark residue was charged with 3 mL of  $Et_2O$  and stirred for 5 min followed by decantation. This procedure was repeated three times at which point the material was dried under vacuum to afford 0.1150 g (0.2631 mmol, 91%) of dark solid product. FTIR (KBr matrix),  $\nu_{max}$  ( $cm^{-1}$ ): 3084 (w), 2971 (w), 2923 (w), 2853 (w), 1705 (m,  $\nu_{CO}$ ), 1579 (s,  $\nu_{NO}$ ,  $\nu_{C=N}$ ), 1545 (s), 1460 (m), 1436 (m), 1382 (s), 1354 (m), 1292 (s), 1271 (s), 1228 (w), 1181 (m), 1115 (m), 1080 (w), 1034 (s), 978 (m), 913 (w), 894 (m), 864 (w), 819 (w), 794 (w), 749 (s), 678 (m), 657 (w), 613 (m), 531 (w), 492 (w), 475 (w), and 448 (w). UV-vis (THF, 298 K),  $\lambda_{max}$ , nm ( $\epsilon$ ,  $M^{-1} cm^{-1}$ ): 371 (24,000), 419 (16,300), and 471 sh (10,300). Anal. calcd for  $C_{16}H_{10}Cl_2FeKN_5O \cdot 1.25 acetone \cdot 0.5 H_2O$ : C, 44.28; H, 3.48; N, 13.07. Found: C, 44.05; H, 3.25; N, 12.83.

### 2.3.12. Synthesis of $K[Fe(LN_4^{PhCl})(NO)]$ (**6-<sup>15</sup>NO**)

The isotopically-labeled complex **6-<sup>15</sup>NO** was prepared analogously to **6** except for using 0.0982 g (0.2366 mmol) of **4-<sup>15</sup>NO** dissolved in 3 mL of acetone and 0.0351 g (0.2597 mmol) of  $KC_8$ . Yield: 0.0951 g (0.2094 mmol, 89%). FTIR,  $\nu_{NO}$  ( $cm^{-1}$ ): obscured due to overlap with  $\nu_{C=N}$ .

## 2.4. Reactivity studies

### 2.4.1. Chemical oxidation of $K[Fe(LN_4^{Ph})(NO)]$ (**5**)

To a 1 mL MeCN solution of complex **5** (0.0225 g, 0.0584 mmol) was added a 1 mL MeCN solution containing 0.0192 g (0.0580 mmol) of ferrocenium hexafluorophosphate ( $FcPF_6$ ). Addition of the oxidant resulted in immediate precipitation of a dark material and the solution color became paler. This heterogeneous solution was stirred for 30 min at RT, which resulted in no further change. The solution was concentrated to dryness and treated with 2 mL of MeOH to separate and yield 0.0178 g (0.0514 mmol, 89%) of the  $\{FeNO\}^7$  complex **3**. The FTIR spectrum (KBr) of this solid is consistent with authentic **3** ( $\nu_{NO}$ : 1698  $cm^{-1}$ ).

### 2.4.2. Chemical oxidation of $K[Fe(LN_4^{PhCl})(NO)]$ (**6**)

This reaction and workup was performed analogously to the oxidation of **5** except for using 0.0409 g (0.0901 mmol) of **6** and 0.0298 g (0.0900 mmol) of  $FcPF_6$ . The addition of  $FcPF_6$  resulted in a burgundy-red insoluble material, which after workup yielded 0.0322 g (0.0776 mmol, 86%) of  $\{FeNO\}^7$  complex **4**. The FTIR spectrum (KBr) of this solid is consistent with authentic **4** ( $\nu_{NO}$ : 1720  $cm^{-1}$ ).

### 2.4.3. UV-vis monitoring of the reaction of $\{FeNO\}^7$ and $\{FeNO\}^8$ compounds with $[Fe(TPP)Cl]$

A 1 mM stock solution of  $[Fe(TPP)Cl]$  in THF was prepared anaerobically and in the dark. Addition of a 0.025 mL aliquot of the  $[Fe(TPP)Cl]$  stock to 2.975 mL of THF resulted in an 8.33  $\mu M$  working solution of  $[Fe(TPP)Cl]$ . After a THF blank was recorded at 298 K, the spectrum of the working solution was recorded. The UV-vis spectrum thus obtained was consistent with literature [50] and was monitored over 15 min resulting in no observable change. To this cuvette was then added a 0.025 mL aliquot of a 1 mM stock of the  $\{FeNO\}^7$  (**3** or **4** in THF) or  $\{FeNO\}^8$  (**5** or **6** in acetone) compounds (1:1 ratio of  $[Fe(TPP)Cl]/\{FeNO\}^{7/8}$ ) to initiate the reaction. The reaction mixture was allowed to equilibrate at 298 K for 1 min and the spectrum was

recorded. Subsequent UV–vis spectra were recorded at 298 K until no further change was observed.

#### 2.4.4. UV–vis monitoring of the reaction of $K[Fe(LN_4^{PhCl})NO]$ (**6**) with $[Fe(TPP)OTf]$

The UV–vis reactions of **6** with  $[Fe(TPP)OTf]$  were performed analogously to those with  $[Fe(TPP)Cl]$  from Section 2.4.3. The  $[Fe(TPP)OTf]$  was obtained by literature methods [51] and compared well to known spectroscopic data including UV–vis (see Fig. S16 in the Supporting information) and FTIR [51,52].

#### 2.4.5. Reaction of $\{FeNO\}^7$ and $\{FeNO\}^8$ compounds with $[Fe(TPP)Cl]$

The bulk reactivity studies were performed using 0.0200 g of  $[Fe(TPP)Cl]$  (0.0284 mmol) and a stoichiometric equivalent of the respective  $\{FeNO\}^7$  (**3**/**3-<sup>15</sup>NO** or **4**/**4-<sup>15</sup>NO**) and  $\{FeNO\}^8$  (**5**/**5-<sup>15</sup>NO** or **6**/**6-<sup>15</sup>NO**) species. A solution of  $[Fe(TPP)Cl]$  was prepared either in 2 mL of THF (for  $\{FeNO\}^7$  complexes **3** or **4**) or 2 mL of THF/acetone (1%) (for  $\{FeNO\}^8$  **5** or **6**) to mimic the UV–vis conditions. To these  $[Fe(TPP)Cl]$  solutions was added a 1 mL THF (**3** or **4**) or THF/acetone (1%) (**5** or **6**) solution containing the  $\{FeNO\}^7$  or  $\{FeNO\}^8$  species, respectively. The reaction was stirred at RT and in the dark for 2 h at which point the solvent was removed in vacuo to afford a dark brown-purple residue, which was characterized by FTIR. Pure  $[Fe(TPP)NO]$  was isolated by treating the brown-purple mixture with ~2 mL of MeOH, which resulted in an isolable product. Example yields: 0.0171 g (0.0243 mmol, 86%) and 0.0186 g (0.0264 mmol, 93%) of purple solid corresponding to  $[Fe(TPP)NO]$  and  $[Fe(TPP)<sup>15</sup>NO]$  from the reaction of  $[Fe(TPP)Cl]$  with **6** and **6-<sup>15</sup>NO**, respectively.

#### 2.5. X-ray crystallographic data collection and structure solution and refinement

Dark-red crystals of  $[Fe(LN_4^{Ph})(NO)]$  (**3**) were grown under anaerobic conditions by slow diffusion of pentane into a toluene solution of **3** at  $-20^\circ\text{C}$ . Suitable crystals were mounted on a glass fiber. All geometric and intensity data were measured at 100 K on a Bruker SMART APEX II CCD X-ray diffractometer system equipped with graphite-monochromatic Mo  $K\alpha$  radiation ( $\lambda = 0.71073 \text{ \AA}$ ) with increasing  $\omega$  (width  $0.5^\circ$  per frame) at a scan speed of 10 s/frame controlled by the SMART software package [53]. The intensity data were corrected for Lorentz-polarization effects and for absorption [54] and integrated with the SAINT software. Empirical absorption corrections were applied to structures using the SADABS program [55]. The structures were solved by direct methods with refinement by full-matrix least-squares based on  $F^2$  using the SHELXTL-97 software [56] incorporated in the SHELXTL 6.1 software package [57]. The atom of O(2) bonded to N(10) on the terminal NO group was found disordered in two sets labeled as O(2) (one set) and O(2') (another set), respectively (see Fig. S1 in the Supporting information). Each of these two sets is divided using the PART commands and proper restraints. The set of O(2) has 60% occupancy while the other O(2') has 40% occupancy. The hydrogen atoms were fixed in their calculated positions and refined using a riding model. All non-hydrogen atoms were refined anisotropically. Selected crystal data and metric parameters for complex **3** are summarized in

Tables 1 and S1 (see the Supporting information). Selected bond distances and angles for one unique molecule of complex **3** are given in Table 1. Perspective views of the complexes were obtained using ORTEP [58]. An ORTEP view of complex **3** showing the disordered O atom is illustrated in Fig. S1.

### 3. Results and discussion

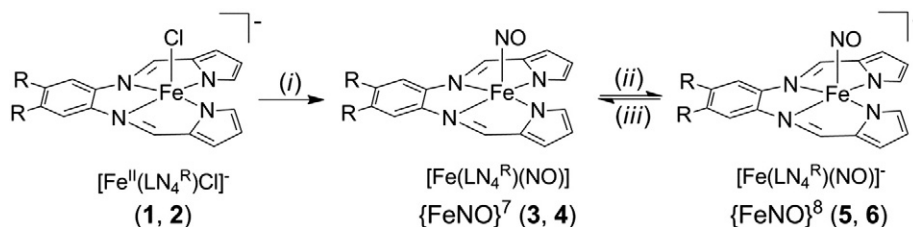
#### 3.1. Synthesis of $\{FeNO\}^7$ complexes

Coordination of HNO or its anion to Fe has been proposed in several heme and non-heme systems as described previously [31,32,34,35,41–44,59]. Although the list is sparse, the collective use of porphyrin and cyclam N-ligands has been a popular choice in the construction of  $\{FeNO\}^8$  complexes. In this regard, we chose to utilize non-macrocyclic but pseudo-planar  $N_4$ -ligand platforms with electronically variable peripheral atoms, denoted as  $LN_4^R H_2$  (H represents dissociable pyrrole protons; R is defined above), for the synthesis of FeNO complexes in this work. The presence of the pyrrolide N-donors in these ligand frames replicates the electronic properties provided by porphyrins/hemes but in a non-macrocyclic i.e. non-heme environment. These ligands thus represent hybrid heme/non-heme constructs that would allow one to achieve  $\{FeNO\}^8$  with the relatively weak  $\pi$ -basic pyrrolide-N, but with the coordination flexibility of a non-heme system. Indeed, such ligands have been used in the construction of high-valent iron-oxos [60,61] and vanadium- $N_2O$  [62] coordination complexes. Collectively, our strategy was to synthesize  $\{FeNO\}^7$  complexes by introduction of NO(g) to Fe(II) precursor complexes, namely  $(Et_4N)[Fe(LN_4^R)Cl]$  (**1** and **2**), and then reduce the  $\{FeNO\}^7$  species (**3** and **4**) chemically or electrochemically to obtain the  $\{FeNO\}^8$  complexes (**5** and **6**, see Scheme 1).

The  $\{FeNO\}^7$  complexes were synthesized by direct NO(g) purge into MeCN solutions of the precursor molecules,  $(Et_4N)[Fe(LN_4^{Ph})Cl]$  (**1**) and  $(Et_4N)[Fe(LN_4^{PhCl})Cl]$  (**2**), to afford  $[Fe(LN_4^{Ph})(NO)]$  (**3**) and  $[Fe(LN_4^{PhCl})(NO)]$  (**4**), respectively, as red-brown solids in ~80% yield at RT (Scheme 1). Complexes **3** and **4** readily precipitated from MeCN upon formation, which allowed for straightforward isolation and purification of the  $\{FeNO\}^7$  product. Particularly, **3** precipitated as a fine microcrystalline solid due to its partial solubility in MeCN, whereas **4** came out of the solution as an amorphous powder with limited MeCN solubility. Complexes **3** and **4** appear to be relatively stable with respect to air or excess NO(g) purge and thus can be handled safely under ambient conditions.

#### 3.2. X-ray crystal structure of $[Fe(LN_4^{Ph})(NO)]$ (**3**)

Single crystals of  $\{FeNO\}^7$  complex **3** were grown from slow diffusion of pentane into a toluene solution of **3** at  $-20^\circ\text{C}$  over the course of 3 days. There are two unique molecules in the asymmetric unit of **3** which are nearly isostructural (Figs. 1 and S1) and their metric parameters are reported below (Table 2) and in the Supporting information (Table S2). No significant close contacts are observed between the molecules; however, there appears to be a weak interaction between the nitrosyl N (N5) of one molecule and the phenyl carbon (C23) of



**Scheme 1.** Synthetic routes for  $\{FeNO\}^{7/8}$  complexes. (i) NO (g), MeCN, RT; (ii)  $KC_8$ , acetone, RT or  $[Co(Cp^*)_2]$ , toluene, RT; (iii)  $FcPF_6$ , MeCN, RT. R groups are defined in Chart 2.

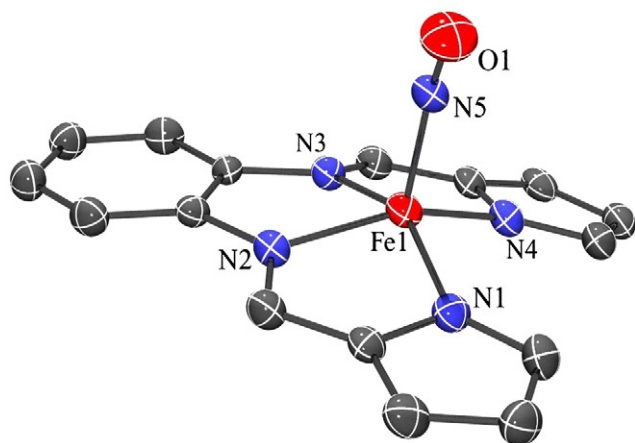


**Fig. 1.** ORTEP diagram of  $[\text{Fe}(\text{LN}_4^{\text{ph}})(\text{NO})]$  (**3**) (one unique molecule) at 50% thermal probability ellipsoids for all non-hydrogen atoms with the atom labeling scheme. Selected bond distances and angles are given in Table 2.

another (N5–C23: 3.125 Å; sum of the van der Waals radii for N and C: 3.25 Å [63]; see Fig. S2) suggestive of  $N_{\pi}$ – $C_{\pi}$  overlap. The Fe center in **3** is coordinated in a square-pyramidal (Sq-Py) geometry from the planar  $[\text{LN}_4^{\text{ph}}]^{2-}$  ligand comprising the basal plane and N-coordinated NO in the axial position (Fig. 1). This polyhedral assignment is demonstrated by a  $\tau$  value of nearly 0 ( $\tau_{\text{avg.}}$  [average of two independent molecules] = 0.025 for **3**), where  $\tau$  is the trigonal distortion parameter as defined by Addison and Reedijk [64]. The metric parameters (Table 2) of the complex are consistent with a LS configuration about the Fe center, especially the Fe–L distances that are all less than 2 Å. The Fe– $N_{\text{imine}}$  bonds (avg.: 1.926 Å) are slightly shorter than the corresponding Fe– $N_{\text{pyrrole}}$  bonds (avg.: 1.966 Å). These distances appear to be a bit contracted, but mostly consistent with other five-coordinate (5C) Sq-Py  $\{\text{FeNO}\}^7$  complexes such as  $[\text{Fe}(\text{TPP})(\text{NO})]$  and  $[\text{Fe}(\text{OEP})(\text{NO})]$ , which display average Fe– $N_{\text{pyrrole}}$  distances of ~2.00–2.01 Å [29,65]. Although the  $N_{\text{pyrrole}}$  is generally considered as a stronger-field ligand than  $N_{\text{imine}}$ , the resulting distances in the structure of **3** presumably arise from the significantly acute bite angle of the phenylenediimine portion of  $\text{LN}_4$  (avg.  $N_{\text{imine}}\text{–Fe–}N_{\text{imine}}$ : 81.89°) versus the more open angle of the  $N_{\text{pyrrole}}\text{–Fe–}N_{\text{pyrrole}}$  (avg.: 104.22°). In contrast, the similarly disposed  $\{\text{FeNO}\}^7$  complex  $[\text{Fe}(\text{LN}_4^{\text{pr}})(\text{NO})]$  (**7**), containing a propyl linker between the diimine donors, displays shorter Fe– $N_{\text{pyrrole}}$  (avg.: 1.945 Å) versus Fe– $N_{\text{imine}}$  (avg.: 1.984 Å) bonds [43]. It is possible that the greater flexibility in the ligand frame of **7** allows for electronic influences of the N-donor to be more representative in the

bond length due to the relaxed and non-conjugated coordination i.e. the  $N_{\text{imine}}\text{–Fe–}N_{\text{imine}}$  (avg.: 90.10°) and  $N_{\text{pyrrole}}\text{–Fe–}N_{\text{pyrrole}}$  (avg.: 95.39°) angles are more ideal. The Fe center in **3** is situated slightly above the plane defined by the four N-ligands of  $\text{LN}_4$  by 0.41 Å and is reflected in the bond angles of trans N-donors (in the basal plane) e.g. N2–Fe1–N4: 152.05°, which are significantly less than the 180° expected for a perfect square-pyramid.

The metric parameters associated with the Fe–N–O unit are often indicative of the nature of the Fe and NO in this highly delocalized bond. Complex **3** displays features that are mostly characteristic of other 5C Sq-Py  $\{\text{FeNO}\}^7$  complexes (vide supra); however, some differences are noted. Analogous to other  $\{\text{FeNO}\}^7$  complexes [29,65–67], the Fe–N (avg.: 1.696 Å) and N–O (avg.: 1.150 Å) distances are short and generally consistent with a LS-Fe(II)–NO• assignment for this complex (vide infra). The Fe–N–O angle in **3** (avg.: 154.4°) is bent from linearity, which is somewhat representative for this class of nitrosyls and reflective of a radical localized on the nitrogen atom of NO and verified by the N-hyperfine coupling to  $g_z$  in the EPR spectrum (vide infra). However, the average Fe–N–O angles in similar LS 5C  $\{\text{FeNO}\}^7$  complexes are more bent (Fe–N–O ~140°) [29,66], ~15° less than the angle found in complex **3**. Thus, complex **3** is certainly an outlier with respect to the Fe–N–O angle. This deviation should be reflected in the  $\nu_{\text{NO}}$  stretching frequency in the IR; however, the IR spectra of **3** and **4** are quite in-line for  $\{\text{FeNO}\}^7$  complexes (vide infra). Indeed, computations by Ghosh [68] and Lehnert [36] for a variety of LS ( $S=1/2$ ) heme and non-heme 5C systems suggest that this linearity is due to significant  $d_z$ – $p_z$  mixing which alleviates repulsion between the  $\sigma$  lone pair on NO and the Fe  $d_z^2$ -based HOMO (highest occupied molecular orbital). The DFT (density functional theory) results by Ghosh revealed a positive correlation between the Fe–N–O angle and the percentage of Fe  $p_z$  in the HOMO and a negative correlation with the Fe–N distance in several theoretical 5C Sq-Py LS  $\{\text{FeNO}\}^7$  derivatives. That is, the larger Fe–N–O angle leads to greater % $p_z$ , less electron repulsion, and greater Fe–N(O) overlap (or contracted Fe–N bond). In using these theoretical results with those experimentally obtained for complex **3** i.e. its Fe–N–O angle of ~155°, one would estimate an 8–9% Fe  $p_z$  character in its HOMO and an Fe–N distance of ~1.68–1.69 Å. The Fe–N distance obtained from the theoretical correlation line fits well with the experimental value. Thus, the independently reported theoretical results have been somewhat validated by our experiments. Accordingly, the more bent angle typically observed in 5C  $\{\text{FeNO}\}^7$  hemes (avg.: 144°) correlates with a ~3–4% Fe  $p_z$ -character in the HOMO and an Fe–N distance of ~1.73 Å (compare with avg.: 1.73 Å from experiment [29,65–67,69]). Taken together, our experiments in combination

**Table 2**

Selected bond distances (Å) and bond angles (deg) for one of the two unique molecules of  $[\text{Fe}(\text{LN}_4^{\text{ph}})(\text{NO})]$  (**3**) as depicted in Fig. 1. See Table S2 and Fig. S1 for metric parameters of the other unique molecule.

$[\text{Fe}(\text{LN}_4^{\text{ph}})(\text{NO})]$ ( <b>3</b> )	
Fe1–N1	1.960(3)
Fe1–N2	1.918(3)
Fe1–N3	1.928(3)
Fe1–N4	1.986(3)
Fe1–N5	1.694(3)
N5–O1	1.150(4)
O1–N5–Fe1	155.6(3)
N1–Fe1–N2	81.97(12)
N1–Fe1–N3	153.72(12)
N1–Fe1–N4	104.40(12)
N1–Fe1–N5	95.90(13)
N2–Fe1–N3	81.84(12)
N2–Fe1–N4	152.05(12)
N2–Fe1–N5	101.41(13)
N3–Fe1–N4	81.36(12)
N3–Fe1–N5	107.51(13)
N4–Fe1–N5	104.87(13)

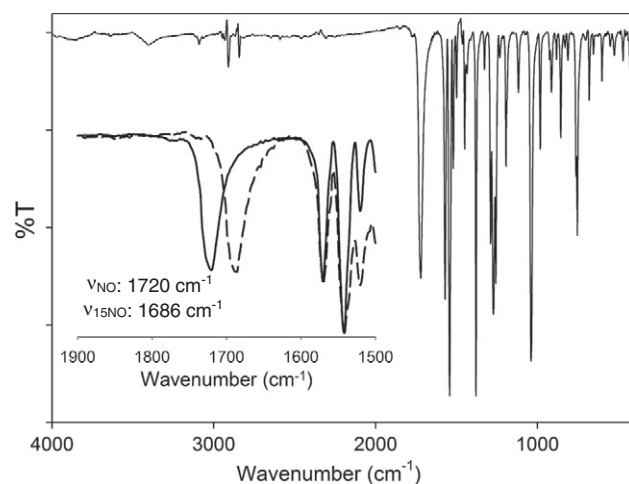


**Fig. 2.** FTIR spectra of  $[\text{Fe}(\text{LN}_4^{\text{phCl}})(\text{NO})]$  (**4**) (solid line) and  $[\text{Fe}(\text{LN}_4^{\text{ph}})(^{15}\text{NO})]$  (**4-<sup>15</sup>NO**) (dashed line; inset) in a KBr matrix.

with theoretical results by others [36,68] suggest that 5C {FeNO}<sup>7</sup> complexes are better described as LS-Fe(I)-NO<sup>+</sup>, likely in resonance with LS-Fe(II)-NO• owing to the highly delocalized nature of this bond.

### 3.3. Spectroscopic and reactive properties of {FeNO}<sup>7</sup> complexes

#### 3.3.1. {FeNO}<sup>7</sup> spectroscopic properties

In addition to the structural characterization of **3**, various spectroscopic measurements on {FeNO}<sup>7</sup> complexes **3** and **4** were performed. Generally, FTIR spectroscopy is employed to gauge the strength of the N–O and M–N(O) bonding in metal-nitrosyls. In particular, the intense N–O stretching frequency ( $\nu_{\text{NO}}$ ) can be particularly informative in MNO systems, but should be interpreted with caution [29]. For example, the solid-state  $\nu_{\text{NO}}$  values for **3** and **4** are observed at 1698 and 1720 cm<sup>-1</sup> (KBr), respectively (Fig. 2 for **4**). These values do not appear to shift significantly in the solution-state for a variety of weakly-/non-coordinating solvents (~1720 cm<sup>-1</sup>), but a red-shift for **4** at ~15 cm<sup>-1</sup> (1705 cm<sup>-1</sup>) in donor solvents such as MeCN and DMSO, indicative of potential solvent coordination in these solutions. Predictably, the  $\nu_{\text{NO}}$  of **4** is blue-shifted from **3** due to the electron withdrawing nature of the peripheral Cl groups on the ligand resulting in decreased Fe  $\pi$ -back-donation into the NO  $\pi^*$  MO [29,36,70]. The average  $\nu_{\text{NO}}$  values for the 5C Sq-Py complexes also appear in this range (1630–1690 cm<sup>-1</sup>) [29,66]. When <sup>15</sup>NO(g) is used in the preparation of **3** and **4**, the  $\nu_{\text{NO}}$  values shift in agreement with the classic harmonic oscillator model,  $\nu_{\text{NO}}$ : 1667 cm<sup>-1</sup> (KBr,  $\Delta\nu_{\text{NO}}$ : 31 cm<sup>-1</sup>) for **3** and  $\nu_{\text{NO}}$ : 1686 cm<sup>-1</sup> (KBr,  $\Delta\nu_{\text{NO}}$ : 34 cm<sup>-1</sup>) for **4** (Fig. 2 for **4**-<sup>15</sup>NO).

The 5C {FeNO}<sup>7</sup> complexes **3** and **4** are paramagnetic and display magnetic properties that are consistent with a doublet electronic ground state ( $S=1/2$ ), which is typical for this class of iron-nitrosyls [29,65]. This assignment has been confirmed by magnetic moment measurements (see Materials and methods) and X-band EPR spectroscopy. For example, EPR measurements (10 K, 3:1 toluene/MeCN) on **3** and **4** reveal an axial feature at  $g\sim 2.07$ – $2.01$  consistent with the high symmetry of these Fe–N<sub>4</sub>–NO complexes (see Supporting information, Fig. S3 for complex **4**). Additionally, hyperfine coupling to the  $I=1$  nucleus of the NO nitrogen with  $A\sim 16$  G is observed in the  $g_z$  component. DFT calculations [36,43] have shown that this hyperfine coupling is actually representative of a minority spin-density localized on N with the majority spin localized on Fe and consistent with an LS-Fe(I)-NO<sup>+</sup> description (vide supra). Complexes **3** and **4** are red-brown in color in organic solvents such as DMF and THF displaying similar UV–vis spectral features with an intense  $\lambda_{\text{max}}\sim 350$  nm and a visible shoulder at ~470 nm. The electronic transitions at 350 and 470 nm have been tentatively assigned as  $\pi$ – $\pi^*$  from the ligand frame and MLCT (metal-to-ligand charge-transfer), respectively. There appears to be little difference in the UV–vis spectrum when the solvent dielectric is changed to DMF indicating that the electronic structure is similar in coordinating and weak-/non-coordinating solvents at least at 298 K.

#### 3.3.2. Electrochemical properties

The electrochemical properties of MNO systems are of principal importance since the general goal of our research is to utilize the changes in the MNO redox levels to access underexplored EF notations in metal-nitrosyls and, more specifically, the {FeNO}<sup>8</sup> state in this contribution. It is therefore a general requirement to construct molecules that display reversible/diffusion-controlled MNO redox couples in order to synthesize an {FeNO}<sup>8</sup> complex from an {FeNO}<sup>7</sup> precursor. Indeed, the cyclic voltammograms (CVs) of **3** and **4** revealed this property. For example, the CV of **3** and **4** in MeCN/RT displayed a reversible  $E_{1/2}$  at  $-1.23$  V ( $\Delta E_p$ : 0.110 V) and  $-1.16$  V ( $\Delta E_p$ : 0.078 V) (both vs. Fc<sup>+</sup>/Fc; or  $-0.83$  and  $-0.76$  V, respectively vs. SCE [71]), respectively (see Figs. 3–4). Differential pulse voltammetry (DPV) further confirmed the CV results (see Figs. 3–4). As expected, the  $E_{1/2}$  for **3** is 70 mV more negative and

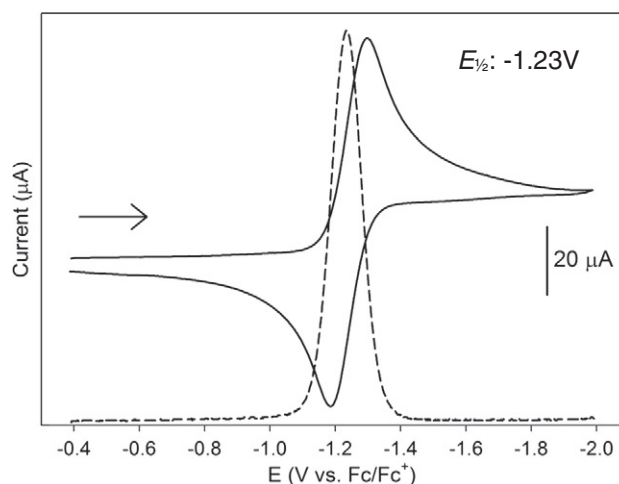


Fig. 3. Cyclic voltammogram (solid line) and differential pulse voltammogram (dashed line) of a 10 mM MeCN solution of [Fe(LN<sub>4</sub><sup>ph</sup>)(NO)]<sup>-</sup> (**3**) (0.1 M nBu<sub>4</sub>NPF<sub>6</sub> supporting electrolyte, glassy carbon working electrode, Pt-wire counter electrode, 100 mV/s scan speed, RT). The arrow displays the direction of the scan.

thus more difficult to reduce than **4** due to the electron-withdrawing nature of the Cl substituents on the ligand. These values compare favorably with the {FeNO}<sup>7</sup>/FeNO<sup>8</sup> redox couples for [Fe(TPP)(NO)] ( $-0.93$  V vs. SCE in CH<sub>2</sub>Cl<sub>2</sub>) and [Fe(OEP)(NO)] ( $-1.08$  V vs. SCE in THF, see Table 1), but are significantly and expectedly more negative than the halogenated FeNO complex [Fe(TFPBr<sub>8</sub>)(NO)] ( $-0.19$  V vs. SCE in CH<sub>2</sub>Cl<sub>2</sub>) (Table 1). The electrochemical results thus confirm that the {FeNO}<sup>8</sup> oxidation state is accessible with minimal structural rearrangement within these ligand architectures.

### 3.4. Synthesis and spectroscopic properties of {FeNO}<sup>8</sup> complexes

#### 3.4.1. Synthesis of {FeNO}<sup>8</sup> complexes

The {FeNO}<sup>8</sup> complexes were synthesized via chemical reduction of the {FeNO}<sup>7</sup> complexes **3** and **4** to generate [Fe(LN<sub>4</sub><sup>ph</sup>)(NO)]<sup>-</sup> (anion of **5**) and [Fe(LN<sub>4</sub><sup>ph</sup>Cl)(NO)]<sup>-</sup> (anion of **6**), respectively, where the cation depends on the reductant used in the synthesis (Scheme 1). In previous accounts by our lab [43] and others [34], this reduction has been accomplished using cobaltocene [Co(Cp)<sub>2</sub>] or decamethylcobaltocene [Co(Cp<sup>\*</sup>)<sub>2</sub>] as reducing agents with the selection being dependent on the potential of the {FeNO}<sup>7</sup>/FeNO<sup>8</sup> redox couple. These metallocene reductants work reasonably well, but the necessity to often purify [Co(Cp<sup>\*</sup>)<sub>2</sub>] and the insolubility of the {FeNO}<sup>8</sup> as the [Co(Cp<sup>\*</sup>)<sub>2</sub>]<sup>+</sup> salt complicated the synthesis. For example, Geiger and Connolly recommend that [Co(Cp)<sub>2</sub>] be sublimed before use, stored in the dark at  $-10$  °C, and used within 10 days [71]. Regardless, reaction of complexes **3** or **4** with [Co(Cp<sup>\*</sup>)<sub>2</sub>] in toluene at RT resulted in respectable yields of the {FeNO}<sup>8</sup> complexes, [Co(Cp<sup>\*</sup>)<sub>2</sub>][Fe(LN<sub>4</sub><sup>ph</sup>)(NO)] (Cp<sup>\*</sup>**5**) and [Co(Cp<sup>\*</sup>)<sub>2</sub>][Fe(LN<sub>4</sub><sup>ph</sup>Cl)(NO)] (Cp<sup>\*</sup>**6**), which precipitated from the reaction medium. The non-methylated [Co(Cp)<sub>2</sub>] would presumably afford a more polar aprotic soluble cobaltocenium salt, but could not be used since it is not strong enough of a reducing agent. Although this synthesis was successful in our hands, the need for constant purification of the metallocene led us to select other chemical reductants. Thus, inspired by classic reagents used in organometallic reactions, we employed potassium graphite (KC<sub>8</sub>) as the reducing agent. Similarly, the {FeNO}<sup>8</sup> complexes K[Fe(LN<sub>4</sub><sup>ph</sup>)(NO)] (**5**) and K[Fe(LN<sub>4</sub><sup>ph</sup>Cl)(NO)] (**6**) were obtained by reaction of stoichiometric KC<sub>8</sub> with acetone solutions of **3** and **4**, respectively. It is important to point out that stoichiometric KC<sub>8</sub> should be employed in the synthesis as excess leads to disparate reactivity and multiple reduced species probably associated with the imine functionality, which is well documented for this reductant [72,73]. The yields are nearly quantitative and the resulting {FeNO}<sup>8</sup>

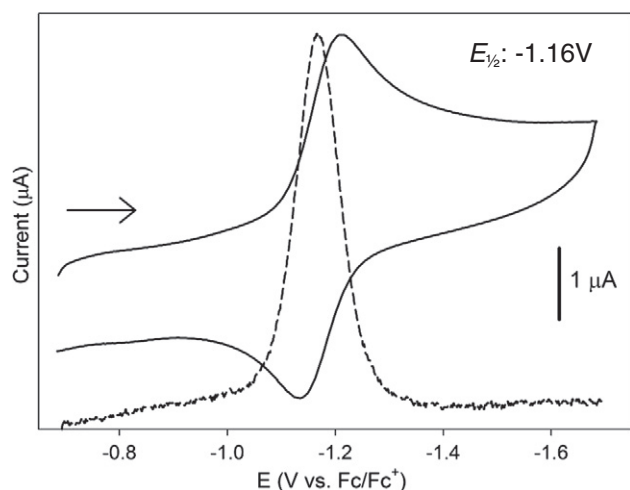


**Fig. 4.** Cyclic voltammogram (solid line) and differential pulse voltammogram (dashed line) of a 1 mM MeCN solution of  $[\text{Fe}(\text{LN}_4^{\text{PhCl}})(\text{NO})]$  (**4**) (0.1 M  $n\text{-Bu}_4\text{NPF}_6$  supporting electrolyte, glassy carbon working electrode, Pt-wire counter electrode, 100 mV/s scan speed, RT). The arrow displays the direction of the scan.

complexes display reasonable solubility in most organic solvents such as MeCN. Additional benefits of this synthetic route include the relative insolubility of the graphite by-product, which is easily separated from the FeNO complex by simple filtration. However, unlike **3** and **4**, compounds **5** and **6** are air-sensitive materials that require anaerobic conditions for workup, storage, and characterization.

#### 3.4.2. $\{\text{FeNO}\}^8$ spectroscopic properties

As described above, vibrational spectroscopy is one of the principal methods of MNO complex characterization, and vibrational measurements on  $\{\text{FeNO}\}^8$  complexes are rare (see Table 2). Additionally, one would expect significant changes in  $\nu_{\text{NO}}$  among  $\{\text{MNO}\}^n$  redox isomers depending on the extent of NO-based redox. Indeed, complexes **5** and **6** display shifted  $\nu_{\text{NO}}$  bands from their parent oxidized complexes **3** and **4**, albeit to a different extent. For example, the solid-state IR spectrum of **5** displayed  $\nu_{\text{NO}}$  at  $1667\text{ cm}^{-1}$  (identified by  $^{15}\text{N}$  isotopic labeling), which is only  $43\text{ cm}^{-1}$  away from the parent  $\{\text{FeNO}\}^7$  complex **3**. This value appears to be more consistent with a ligand-based reduction instead of  $\{\text{FeNO}\}$  unit reduction although this result may be more indicative of a thermally accessible triplet excited state (vide infra). A ligand based reduction would not be too surprising given the highly delocalized nature of the  $\text{LN}_4$  scaffold, which is evidenced by the

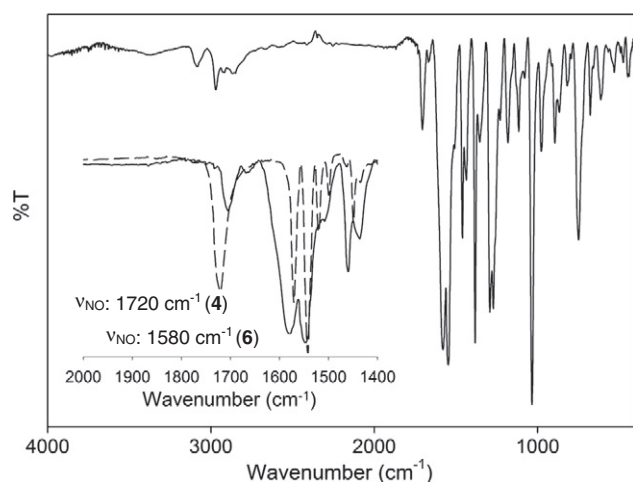


**Fig. 5.** FTIR spectra of  $\text{K}[\text{Fe}(\text{LN}_4^{\text{PhCl}})(\text{NO})]$  (solid line) (**6**) and  $[\text{Fe}(\text{LN}_4^{\text{PhCl}})(\text{NO})]$  (dashed line; inset) (**4**) in a KBr matrix. The peak at  $1705\text{ cm}^{-1}$  in **6** represents coordinated acetone  $\nu_{\text{CO}}$ .

disparate C–C bond distances in the X-ray structure especially in the pyrrolide ring (see Table S1). The  $\nu_{\text{NO}}$  band of **6**; however, shifted significantly from parent **4** ( $1720\text{ cm}^{-1}$ ) to  $\sim 1580\text{ cm}^{-1}$  (approximate due to overlap with  $\text{LN}_4$   $\nu_{\text{C}=\text{N}}$  bands, see Fig. 5). Both **5** and **6** also display  $\nu_{\text{CO}}$  values at  $1705\text{ cm}^{-1}$  that are similar to metal-coordinated acetone complexes ( $\nu_{\text{CO}}$ :  $1660\text{--}1700\text{ cm}^{-1}$ ) [74]. The presence of acetone was also confirmed by elemental analysis (see Materials and methods) and mass spectrometry measurements (vide infra). Analogous to other  $\{\text{FeNO}\}^8$  complexes [34], the  $\nu_{\text{NO}}$  is obstructed from ligand vibrational bands. The  $\nu_{\text{NO}}$  value for **6** thus supports reduction in the FeNO unit due to increased occupancy of  $\pi^*$  orbitals on NO from its  $\{\text{FeNO}\}^7$  precursor **4**. These values are also consistent with other heme  $\{\text{FeNO}\}^8$  complexes that have been synthesized or studied by high-level DFT calculations (see Table 1). They are, however, quite higher than the corresponding values for non-heme  $\{\text{FeNO}\}^8$  systems (avg.:  $1300\text{ cm}^{-1}$ ) suggesting that the electronic nature of the  $\text{LN}_4$  frame in **6** is more heme-like.

High-resolution FTMS (HRMS) studies were also performed to confirm the identity of the  $\{\text{FeNO}\}^8$  complexes. Single crystals of such systems have been difficult to grow due to the reactive nature of these complexes (vide infra). As such, no small molecule  $\{\text{FeNO}\}^8$  complex to date (2012) has been characterized by X-ray crystallography or X-ray absorption (XAS) studies although the  $\{\text{FeHNO}\}^8$  analogue of myoglobin has been reported based on XAS [38,40]. Thus, HRMS would provide further confirmation of these elusive metal nitrosyls. The HRMS (negative ion mode) experiments do provide such evidence, as the molecular ion peak  $[\text{M}]^-$  for **5** ( $m/z$ : 346.0385; calcd: 346.0386) does appear with the appropriate isotope pattern (see Supporting information). Complex **6**, on the other hand, only displayed peaks consistent with  $[\text{M} + \text{acetone}]^-$  ( $m/z$ : 472.0000; calcd: 472.0026) and  $[\text{M} + \text{acetone} - \text{H}]^-$  ( $m/z$ : 470.9967; calcd: 470.9947) with the latter being the predominant species. The  $^{15}\text{N}$  isotopomers were also examined and support the formulation predicted. To the best of our knowledge, the MS studies on the Fe- $\text{LN}_4$ -NO systems [43] represent the only MS measurements performed on such FeNO complexes.

Other spectroscopic methods were employed to characterize complexes **5** and **6**. Both **5** and **6** demonstrate excellent solubility in a variety of organic solvents such as acetone, MeCN, and DMF affording red-brown colored solutions; moderate solubility is observed in non-polar solvents such as THF. The UV-vis spectrum of the  $\{\text{FeNO}\}^8$  complex **6** is similar in shape to  $\{\text{FeNO}\}^7$  complex **4** with some minor changes (Fig. 6). To date (2012), all reported non-heme  $\{\text{FeNO}\}^8$  complexes have been reported as diamagnetic; however, this description represents a small sample size ( $N=2$ ) as the majority of these systems have only been characterized in situ. This property suggests that, if we assign the coordinated NO as a nitroxyl anion, the LS-Fe(II)- $^1\text{NO}^-$  would be the favorable assignment for  $\{\text{FeNO}\}^8$ . Complex **6** displays a complex  $^1\text{H}$  NMR spectrum that is consistent with a diamagnetic system (see Supporting information). The complexity presumably arises from ligation/deligation of solvent (vide infra) or structural rearrangement of the  $\text{LN}_4$  ligand around the Fe center. In contrast, the  $^1\text{H}$  NMR of **5** is observable, but appears broad in nature and consistent with a paramagnetic material. The NMR broadness is attributed to formation of an unknown paramagnetic species upon complex dissolution and/or a thermally accessible higher spin-state (i.e.  $^3\text{NO}^-$  versus  $^1\text{NO}^-$  or ligand reduction). We favor this description since the  $\nu_{\text{NO}}$  of **5** matches quite well with the calculated  $\nu_{\text{NO}}$  values for 6C  $\{\text{FeNO}\}^8$  complexes, which range from  $1612$  to  $1777\text{ cm}^{-1}$  for  $[\text{Fe}(\text{P})(\text{Im})(\text{NO})]^-$  complexes in the  $S=1$  state [36,37]. Additionally, a paramagnetic triplet ground state has been assigned to the  $\{\text{FeNO}\}^8$  adduct of the non-heme TauD system suggesting that higher spin manifolds may be accessible for **5** [44]. Although the extra stability of the  $\{\text{FeNO}\}^8$  in **6** is not quite significant from an electrochemical vantage point ( $\sim 100\text{ mV}$ ), perhaps the presence of the Cl substituents lowers the energy of the ligand  $\pi$ -orbitals just enough to prevent parallel spin occupation and/or ligand reduction. Collectively, it appears that

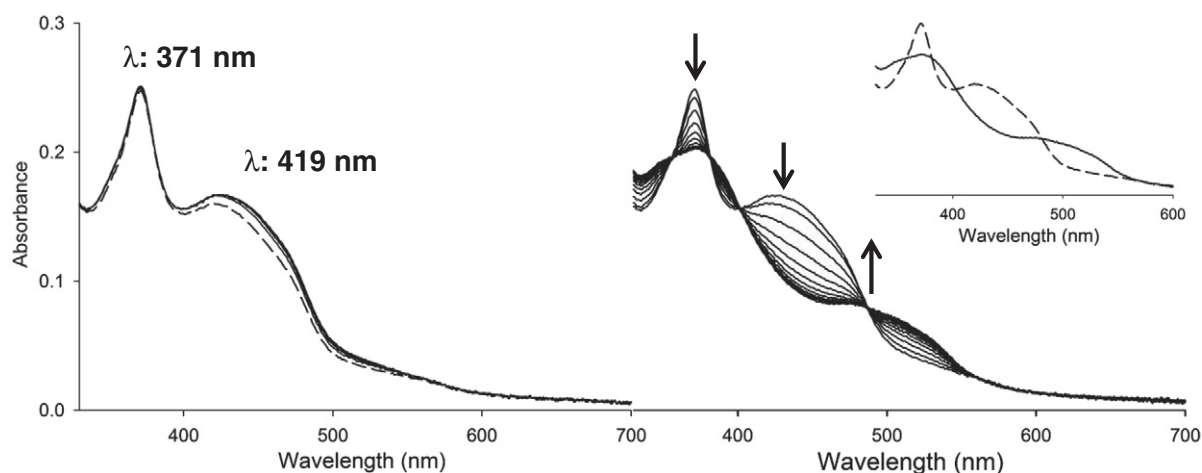


**Fig. 6.** UV-vis spectral monitor of an 8.33  $\mu\text{M}$  THF solution of  $\text{K}[\text{Fe}(\text{LN}_4^{\text{PhCl}})(\text{NO})]$  (**6**) at 298 K. Left: UV-vis monitor of **6** upon initial dissolution (dashed line) and subsequent traces (solid lines) for 15, 30, 45, and 60 min thereafter. Right: continuation of spectral monitor on the left only at 1 h intervals (total time = 12 h); inset depicts the first (dashed line) and last (solid line) scans. Arrows illustrate the direction of change.

heme-based  $\{\text{FeNO}\}^8$  complexes and **6** display  $\nu_{\text{NO}}$ : 1500–1600  $\text{cm}^{-1}$  and generally prefer to be ground state singlets. However, non-heme  $\{\text{FeNO}\}^8$  systems (excluding the examples reported here and elsewhere [43]) display  $\nu_{\text{NO}}$  ~ 1300  $\text{cm}^{-1}$ . This data suggests an oxidation state assignment of  $\text{LS-Fe(II)}-^1\text{NO}^-$  for the non-heme  $\{\text{FeNO}\}^8$  and more of a resonance  $\text{LS-Fe(II)}-^1\text{NO}^- \leftrightarrow \text{LS-Fe(I)}-\text{NO}^\bullet$  description for the heme  $\{\text{FeNO}\}^8$ .

### 3.5. Reactivity of $\{\text{FeNO}\}^7$ and $\{\text{FeNO}\}^8$ complexes

The reactivity of  $\{\text{FeNO}\}^8$  complexes have received little attention with the exception of the protonation studies by Doctorovich on  $[\text{Fe}(\text{TFPPBr}_8)(\text{NO})]^-$  [34], which was shown to liberate  $\text{H}_2(\text{g})$  and reform the  $\{\text{FeNO}\}^7$  complex via a transient  $\{\text{FeHNO}\}^8$  complex. As the reactivity of  $\{\text{FeNO}\}^8$  systems is underexplored and of fundamental importance with respect to the biological fate of  $\text{HNO}/\text{NO}^-$ , we have initiated such reactivity studies in the present contribution. Due to principal reduction of the  $\{\text{FeNO}\}$  unit in **6**, the majority of our reactivity discussion is focused on this system; however, reactions with **5** (a complex more consistent with ligand-based reduction or paramagnetic spin-state) were also performed and resulted in nearly parallel outcomes.

In the absence of structural characterization of **5** or **6** and to support the electrochemical results, the conversion of the  $\{\text{FeNO}\}^8$  complexes back to their oxidized  $\{\text{FeNO}\}^7$  counterparts was performed. For instance, treatment of a MeCN solution of the  $\{\text{FeNO}\}^8$  complexes **5** or **6** with a stoichiometric amount of ferrocenium hexafluorophosphate resulted in quantitative formation of the corresponding  $\{\text{FeNO}\}^7$  complexes **3** and **4** as monitored by FTIR spectroscopy. The reversibility of the FeNO redox states is depicted in Scheme 1. Thus, the  $\{\text{FeNO}\}^{7/8}$  complexes (**3/5** or **4/6**) are chemically and electrochemically interconvertible.

The difficulty in the isolation of single crystals of  $\{\text{FeNO}\}^8$  derivatives is likely derived from the inherent reactivity of these systems. For example, Kadish and Olson reported that exhaustive electrolysis of the  $\{\text{FeNO}\}^8$  complex of TPP simply resulted in isolation of the starting  $\{\text{FeNO}\}^7$  species [33]. This outcome is likely due to the presence of some protic material in the non-polar  $\text{CH}_2\text{Cl}_2$  solvent that resulted in the reaction of  $\text{H}^+$  with the formed  $\{\text{FeNO}\}^8$  complex in an analogous fashion to what is observed by Doctorovich [34]. The inherent reactivity of this class of iron-nitrosyls at least provides some explanation for the lack of isolable  $\{\text{FeNO}\}^8$  complexes in the literature. Previously, our group reported that the structurally similar  $\{\text{FeNO}\}^8$  complex **7** undergoes disproportionation reactions in MeCN or THF to yield the  $\{\text{FeNO}\}^7$  complex and an  $\text{Fe(I)}-\text{N}_2$  species. This

reaction takes nearly 13 h to go to completion [43]. Thus, complex **7** could still be used as a potential nitroxyl donor provided that release of nitroxyl is faster than the disproportionation. We hypothesized that this reaction may be a common feature for  $\{\text{FeNO}\}^8$  species at least with the  $\text{LN}_4$  type of ligand platform. As expected, when a THF solution of **6** was monitored by UV-vis spectroscopy (298 K), distinct changes in the visible region were observed with a decrease in the  $\lambda_{\text{max}}$  at 371 and 419 nm and new bands appearing at  $\lambda_{\text{max}}$  of 361 and 481 nm over the course of 9 h (Fig. 6). Complex **6** is thus more reactive than **7**. There appears to be little change in the UV-vis over the course of ~2 h indicating modest solution stability of the  $\{\text{FeNO}\}^8$  complex (Fig. 6). Additionally, several isosbestic points are present in the spectrum during this process at 359, 384, 403 and 490 nm supporting a clean transformation with the final trace displaying bands at 361 and 481 nm, which appear to be indicative of the  $\{\text{FeNO}\}^7$  complex **4**. FTIR analysis of this reaction also revealed the  $\nu_{\text{NO}}$  bands of **4**, which further confirmed the formation of the  $\{\text{FeNO}\}^7$  complex. Further examination of the UV-vis experiments indicates that  $\{\text{FeNO}\}^7$  **4** is obtained in a quantitative yield, which eliminates a disproportionation reaction. This result suggests that a simple oxidation is taking place over prolonged storage of **6** in solution to result in **4** and reduction of the solvent. Another path to obtain

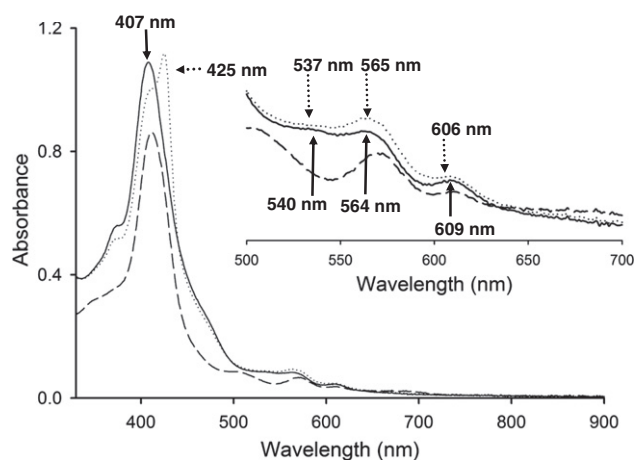
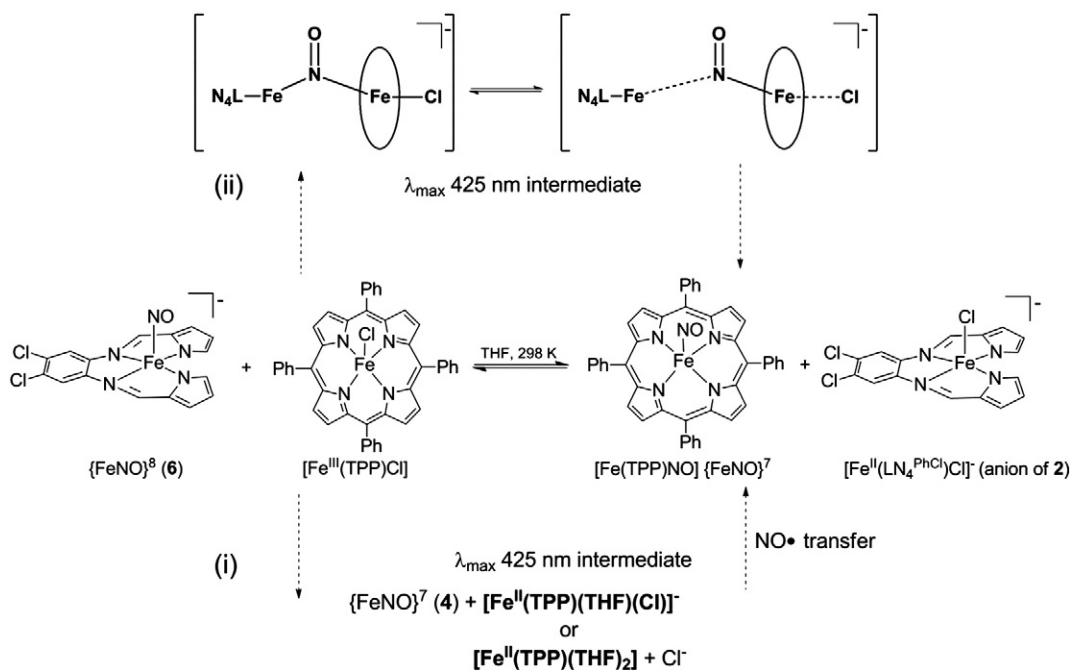


**Fig. 7.** UV-vis spectrum of an 8.33  $\mu\text{M}$  THF solution of  $[\text{Fe}(\text{TPP})\text{Cl}]$  (dashed line), 1 min after (dotted line), and 1 h after (solid line) the addition of 1 mol-equiv of  $\text{K}[\text{Fe}(\text{LN}_4^{\text{PhCl}})(\text{NO})]$  (**6**) at 298 K. Inset: expansion of the Q-band region of the spectrum. Arrows are coded according to the spectrum they represent.

{FeNO}<sup>7</sup> from {FeNO}<sup>8</sup> would be via protonation as demonstrated by Doctorovich [34] as described above; however, this reaction seems unlikely under the anhydrous/anaerobic conditions employed. Complex **5** also undergoes a similar reactivity profile in THF but appears to form the {FeNO}<sup>7</sup> species more rapidly (6 h).

The established reductive nitrosylation [75] reaction of HNO with ferric hemes is among the most sensitive chemical tests for HNO-releasing molecules where HNO provides both the electron and NO to form an {FeNO}<sup>7</sup> ferrous-NO heme [39,76,77]. Additionally, M(III)-porphyrin complexes have been demonstrated as efficient traps for HNO [76,78,79]. To test whether complexes such as **6** could react in a similar manner, we explored the interaction of these {FeNO}<sup>8</sup> complexes with the ferric heme analogue [Fe(TPP)Cl] under dark conditions to prevent any ill-defined photochemistry. The reaction of a THF solution of [Fe(TPP)Cl] at 298 K with stoichiometric amounts of the {FeNO}<sup>8</sup> complexes was monitored by UV–vis and IR spectroscopies. Addition of the {FeNO}<sup>8</sup> complex **6** to [Fe(TPP)Cl] (1:1 ratio) resulted in several changes in the UV–vis spectrum, which are ultimately consistent with the formation of the {FeNO}<sup>7</sup> porphyrin complex, [Fe(TPP)NO], after ~1 h (Fig. 7). The trace after 1 min addition of **6** was a red-shift in the Soret band of [Fe(TPP)Cl] from 412 nm to 425 nm with a significant increase in absorbance. Spectral changes such as this have been attributed to several transformations of [Fe(TPP)Cl]. For example, a similar shift has been observed in the photo-reduction of [Fe(TPP)Cl] in MeOH to form what is assigned as the 6C bis-solvato complex, [Fe(TPP)(MeOH)<sub>2</sub>] [80,81]. While a reduced solvato species is possible in the reported reaction, we must note that the 6C complex described above was formed in MeOH and is only stable on the millisecond timescale. In contrast, these reactions were performed in weakly coordinating THF and the λ<sub>max</sub>: 425 nm species is observed on the minute timescale. Authentic [Fe<sup>II</sup>(TPP)] has been prepared in THF by Darensbourg and coworkers where they report a Soret λ<sub>max</sub> of 412 nm [82]; however, Scheidt and coworkers report the Soret of [Fe<sup>II</sup>(TPP)(THF)<sub>2</sub>] at 425 nm in THF [83]. Therefore, a possible mechanism involving electron transfer from **6** to transiently form a 6C [Fe<sup>II</sup>(TPP)(THF)(Cl)]<sup>-</sup> or [Fe<sup>II</sup>(TPP)(THF)<sub>2</sub>] species cannot be excluded. This step would be followed by NO• transfer from the resulting {FeNO}<sup>7</sup> complex **4** to the ferrous porphyrin to furnish the [Fe(TPP)

NO] complex (Scheme 2, path i). Alternatively, this spectral change to 425 nm may suggest the formation of other transient 6C {FeNO}<sup>7</sup>-porphyrin complexes. In fact, the 6C complex, [Fe(TPP)(NO)(MI)], prepared by Lehnert's group [69] has a Soret absorption band at 425 nm and Q-bands at 538 and 600 nm in CH<sub>2</sub>Cl<sub>2</sub>. The intermediate formed here displays λ<sub>max</sub> at 425, 537, and 606 nm, which is slightly red-shifted and more intense from the final trace with λ<sub>max</sub> at 407, 540, and 609 nm and in-line with authentic [Fe(TPP)NO] (λ<sub>max</sub>: 408, 536, 607 nm in THF [31]). Support for the 6C-NO porphyrin path is found in the Q-band region (Fig. 7). Accordingly, if initial one-electron reduction of [Fe(TPP)Cl] to [Fe(TPP)(THF)(Cl)]<sup>-</sup> or [Fe(TPP)(THF)<sub>2</sub>] is to occur, then this region would change noticeably compared to that of [Fe(TPP)Cl] [84]. The UV–vis experiments show that the Q-band region is essentially unchanged after the first scan (1 min after mixing), whereas the Soret continues to shift over 1 h toward the 407 nm band indicative of [Fe(TPP)NO]. This observation further implicates a 6C-NO porphyrin as the first step in the reductive nitrosylation. When [Fe(TPP)OTf] was prepared [51] and subjected to the same conditions used for [Fe(TPP)Cl] and **6**, a similar 426 nm band is observed in the first spectral trace. Though the OTf<sup>-</sup> anion is considered to be a weaker field ligand than Cl<sup>-</sup>, previous reports describe [Fe(TPP)OTf] as a 5C species instead of an ion pair [51,52]. Since the resulting UV–vis spectral changes were nearly identical to that of compound **6** with [Fe(TPP)Cl], we propose that the net NO<sup>-</sup> transfer is occurring through a similar mechanism with both 5C ferric porphyrins. Thus, a potential mechanism could involve the formation of a binary complex where the NO ligand of **6** bridges the two reactants to form a [P–Fe(μNO)Fe–L]<sup>-</sup> intermediate (Scheme 2, path ii). This species is comparable to the intermediate observed in the transnitrosation of thiolates with nitrosothiols (RSNO) where attack of the nucleophilic thiolate anion on the electrophilic RSNO produces the anionic RSN(O)SR<sup>-</sup> intermediate [85,86]. This type of NO-transfer has been postulated to be involved in safe NO-trafficking, which never involves the release of free NO. By analogy, the process described here would be defined as a “transnitroxylation” where the coordinated NO<sup>-</sup> is transferred from one molecule to another without involving free NO<sup>-</sup>. Electron transfer and nitrosylation take place through the bridge i.e. an inner-sphere mechanism and the 6C



**Scheme 2.** Proposed reaction path (i = electron transfer vs. ii transnitroxylation) intermediates (bracketed and bolded) in the reaction of {FeNO}<sup>8</sup> complex with [Fe<sup>III</sup>(TPP)Cl]. The oval represents porphyrin in the intermediate complex. A similar reaction path is proposed with [Fe<sup>III</sup>(TPP)OTf] (see Fig. S17).

intermediate decays to yield the more stable 5C [Fe(TPP)NO] complex and **2** perhaps via a monomeric [Fe<sup>II</sup>(TPP)(NO)Cl] complex after splitting the bridge (see Scheme 2). The identity of the 425 nm band could be any of these 6C FeNO intermediates. Therefore, the net reaction would be: [Fe(LN<sub>4</sub><sup>R</sup>)(NO)]<sup>-</sup> (anion of **6**) + [Fe(TPP)Cl] → [Fe(TPP)NO] + [Fe(LN<sub>4</sub><sup>R</sup>)Cl]<sup>-</sup> (anion of **2**). Further support for this chemistry comes from IR analysis. The FTIR spectrum of the bulk reaction mixture of [Fe(TPP)Cl]/complex **6** (1:1) confirmed this postulate and the only  $\nu_{\text{NO}}$  bands observed are from [Fe(TPP)NO] ( $\nu_{\text{NO}}$ : 1701 cm<sup>-1</sup> in KBr), which shifted when **6**-<sup>15</sup>N<sub>2</sub> was used ( $\nu_{\text{NO}}$ : 1669 cm<sup>-1</sup> in KBr) (see the Supporting information). Furthermore, the UV-vis spectrum of independently-prepared complex **2** and [Fe(TPP)NO] (mixed in a 1:1 ratio) in THF at 298 K nearly resembles the final spectrum of the reaction described above (see Supporting information). The control reaction of [Fe(TPP)Cl] with the {FeNO}<sup>7</sup> complexes **3** and **4** also appears to generate [Fe(TPP)NO]; however, the reaction time is long (>12 h) and incomplete according to IR and UV-vis spectroscopies. Additionally, Darensbourg observes a similar reaction of [Fe(TPP)Cl] or [Fe(OEP)Cl] with a 5C {FeNO}<sup>7</sup>-N<sub>2</sub>S<sub>2</sub> complex that also takes place over a similar (24–72 h) timescale [82]. Thus, while {FeNO}<sup>7</sup> can ultimately result in the same product as with {FeNO}<sup>8</sup> (**5** and **6**) and dinitrosyl iron complexes (DNICs, the reactions studied by Darensbourg), the reaction path appears very different.

#### 4. Conclusions

The following are the summary of the main findings of this work:

- (i) We have described the synthesis and characterization of several non-heme FeNO complexes supported by the planar LN<sub>4</sub> diimine-dipyrroliide ligand framework, which represent new examples of the {FeNO}<sup>7</sup> (**3** and **4**) and {FeNO}<sup>8</sup> (**5** and **6**) classes of metal nitrosyls in hybrid heme architectures. The synthesis of the rare {FeNO}<sup>8</sup>-type complexes **5** and **6** could be achieved by stoichiometric chemical reduction with [Co(Cp<sup>\*</sup>)<sub>2</sub>] or KC<sub>8</sub>. These {FeNO}<sup>8</sup> species add to the small list of this type of FeNO complex that can be isolated under standard lab conditions.
- (ii) The {FeNO}<sup>7</sup> complexes display spectroscopic and structural properties that are mostly consistent with other 5C FeNO species in this class. One particular outlying feature was demonstrated in the X-ray crystal structure of **3**, which afforded an atypical Fe–N–O angle of ~155° for this EF-notation. This unusual metric parameter has been explained with respect to the relative amount of Fe *p<sub>z</sub>* character in the largely *d<sub>z<sup>2</sup></sub>*-based HOMO of this and similarly disposed 5C {FeNO}<sup>7</sup> complexes. Independent calculations by another group have assigned the oxidation states in such systems as LS-Fe(I)–NO<sup>+</sup> (*S* = 1/2) with a majority spin-density on Fe.
- (iii) The electrochemical properties of {FeNO}<sup>7</sup> complexes **3** and **4** are fairly similar exhibiting reversible and diffusion-controlled redox potentials for the {FeNO}<sup>7/8</sup> couple at –1.23 and –1.16 V (vs. Fc/Fc<sup>+</sup> in MeCN), respectively. The electrochemical data highlight the accessibility and stability of {FeNO}<sup>8</sup> from suitable {FeNO}<sup>7</sup> precursor molecules.
- (iv) Consistent with the electrochemical picture obtained, chemical reduction to obtain {FeNO}<sup>8</sup> complexes **5** and **6** was relatively straightforward if some precaution is followed. This reduction is also reversible and the corresponding {FeNO}<sup>7</sup> complexes **3** and **4** could be re-obtained with ferrocenium oxidants. Complex **5** afforded a  $\nu_{\text{NO}}$  value of ~50 cm<sup>-1</sup> less than the parent {FeNO}<sup>7</sup> complex **3**, which is suggestive of a ligand-based reduction/higher spin-state derivative. Other measurements (NMR) are consistent with this assessment. Complex **6**, on the other hand, afforded a  $\nu_{\text{NO}}$  red-shift of ~140 cm<sup>-1</sup> to 1580 cm<sup>-1</sup> from **4** that was more consistent with {FeNO} unit reduction.

- (v) These air-sensitive {FeNO}<sup>8</sup> materials appear to be indefinitely stable in the solid-state when stored under anaerobic/anhydrous conditions in the dark. Their solution-state solubility is different resulting in slow re-oxidation to the {FeNO}<sup>7</sup> derivatives **3** and **4** over the course of 6–9 h in both polar and apolar organic solvents. The ultimate explanation behind this reactivity is unknown at present, but it is consistent with the label for this class of FeNO systems as “elusive”. However, it is important to point out that these are slow processes with respect to the potential for such molecules to serve as HNO sources.
- (vi) Finally, complexes **5** and **6** exhibit a nitroxyl-like reactivity with the ferric porphyrin complex, [Fe(TPP)Cl], to afford [Fe(TPP)NO] in stoichiometric yield. UV-vis monitoring of this reaction suggests that a potential 6C {FeNO}<sup>7</sup> is an intermediate traversed in the reaction path which may occur through a “transnitroxylation” process.

In sum, unraveling the chemistry of iron-nitroxyl/{FeNO}<sup>8</sup> derivatives is challenging as they represent synthetic targets that are difficult to achieve and maintain. Once stabilized, at least to some extent, they offer new avenues of MNO reactivity that have never been explored. To the best of our knowledge a “transnitroxylation” process has not been proposed before (in stark contrast to transnitrosation), presumably due to a lack of reasonably well-characterized and stable Fe-nitroxyl systems. We expect that systems like these and others will ultimately be used as synthetic analogues of biological Fe-nitroxyls and HNO-donors with therapeutic application.

#### Acknowledgments

T.C.H. acknowledges the NSF, the University of Georgia Research Foundation (UGARF), and the University of Georgia Chemistry Department for funding this research. We also wish to thank Prof. Michael K. Johnson for his assistance with EPR spectroscopy, and Prof. I. Jonathan Amster and Mrs. Melissa Stoudemayer for their help with the high-resolution mass spectral studies.

#### Appendix A. Supplementary data

Supplementary data to this article can be found online at <http://dx.doi.org/10.1016/j.jinorgbio.2012.08.026>.

#### References

- [1] K.M. Miranda, *Coord. Chem. Rev.* 249 (2005) 433–455.
- [2] M.D. Bartberger, W. Liu, E. Ford, K.M. Miranda, C. Switzer, J.M. Fukuto, P.J. Farmer, D.A. Wink, K.N. Houk, *Proc. Natl. Acad. Sci. U. S. A.* 99 (2002) 10958–10963.
- [3] J.C. Irvine, R.H. Ritchie, J.L. Favalaro, K.L. Andrews, R.E. Widdop, B.K. Kemp-Harper, *Trends Pharmacol. Sci.* 29 (2008) 601–608.
- [4] K.M. Miranda, N. Paolucci, T. Katori, D.D. Thomas, E. Ford, M.D. Bartberger, M.G. Espey, D.A. Kass, M. Feelisch, J.M. Fukuto, D.A. Wink, *Proc. Natl. Acad. Sci. U. S. A.* 100 (2003) 9196–9201.
- [5] N. Paolucci, T. Katori, H.C. Champion, M.E. St. John, K.M. Miranda, J.M. Fukuto, D.A. Wink, D.A. Kass, *Proc. Natl. Acad. Sci. U. S. A.* 100 (2003) 5537–5542.
- [6] D.A. Wink, K.M. Miranda, T. Katori, D. Mancardi, D.D. Thomas, L. Ridnour, M.G. Espey, M. Feelisch, C.A. Colton, J.M. Fukuto, P. Pagliaro, D.A. Kass, N. Paolucci, *Am. J. Physiol. Heart Circ. Physiol.* 285 (2003) H2264–H2276.
- [7] H.T. Nagasawa, E.G. DeMaster, B. Redfern, F.N. Shirota, D.J.W. Goon, *J. Med. Chem.* 33 (1990) 3120–3122.
- [8] H.T. Nagasawa, S.P. Kawle, J.A. Elberling, E.G. DeMaster, J.M. Fukuto, *J. Med. Chem.* 38 (1995) 1865–1871.
- [9] M.P. Doyle, S.N. Mahapatro, R.D. Broene, J.K. Guy, *J. Am. Chem. Soc.* 110 (1988) 593–599.
- [10] J. Turk, J.A. Corbett, S. Ramanadham, A. Bohrer, M.L. McDaniel, *Biochem. Biophys. Res. Commun.* 197 (1993) 1458–1464.
- [11] P.S.-Y. Wong, J. Hyun, J.M. Fukuto, F.N. Shirota, E.G. DeMaster, D.W. Shoeman, H.T. Nagasawa, *Biochemistry* 37 (1998) 5362–5371.
- [12] P.J. Farmer, F. Sulc, *J. Inorg. Biochem.* 99 (2005) 166–184.
- [13] M.R. Kumar, J.M. Fukuto, K.M. Miranda, P.J. Farmer, *Inorg. Chem.* 49 (2010) 6283–6292.
- [14] K.M. Miranda, T. Katori, C.L. Torres de Holding, L. Thomas, L.A. Ridnour, W.J. McLaren, S.M. Cologna, A.S. Dutton, H.C. Champion, D. Mancardi, C.G. Tocchetti,

- J.E. Saavedra, L.K. Keefer, K.N. Houk, J.M. Fukuto, D.A. Kass, N. Paolucci, D.A. Wink, J. Med. Chem. 48 (2005) 8220–8228.
- [15] K.M. Miranda, R.W. Nims, D.D. Thomas, M.G. Espey, D. Citrin, M.D. Bartberger, N. Paolucci, J.M. Fukuto, N. Feelisch, D.A. Wink, J. Inorg. Biochem. 93 (2003) 52–60.
- [16] F. Doctorovich, D. Bikiel, J. Pellegrino, S.A. Suárez, A. Larsen, M.A. Martí, Coord. Chem. Rev. 255 (2011) 2764–2784.
- [17] J.M. Fukuto, A.S. Dutton, K.N. Houk, ChemBioChem 6 (2005) 612–619.
- [18] B.A. Averill, Chem. Rev. 96 (1996) 2951–2964.
- [19] A. Daiber, T. Nauser, N. Takaya, T. Kudo, P. Weber, C. Hultschig, H. Shoun, V. Ullrich, J. Inorg. Biochem. 88 (2002) 343–352.
- [20] W.G. Zumft, J. Inorg. Biochem. 99 (2005) 194–215.
- [21] M.P. Schopfer, J. Wang, K.D. Karlin, Inorg. Chem. 49 (2010) 6267–6282.
- [22] V. Shafirovich, S.V. Lymar, Proc. Natl. Acad. Sci. U. S. A. 99 (2002) 7340–7345.
- [23] K.M. Miranda, H.T. Nagasawa, J.P. Toscano, Curr. Top. Med. Chem. 5 (2005) 649–664.
- [24] A. Angeli, A. Angelico, F. Scurti, Chem. Zentralbl. 73 (1902) 691–693.
- [25] A. Angeli, Gazz. Chim. Ital. 33 (1903) 245–252.
- [26] N. Paolucci, M.I. Jackson, B.E. Lopez, K. Miranda, C.G. Tocchetti, D.A. Wink, A.J. Hobbs, J.M. Fukuto, Pharmacol. Ther. 113 (2007) 442–458.
- [27] D. Andrei, D.J. Salmon, S. Donzelli, A. Wahab, J.R. Klose, M.L. Citro, J.E. Saavedra, D.A. Wink, K.M. Miranda, L.K. Keefer, J. Am. Chem. Soc. 132 (2010) 16526–16532.
- [28] D.A. Guthrie, N.Y. Kim, M.A. Siegler, C.D. Moore, J.P. Toscano, J. Am. Chem. Soc. 134 (2012) 1962–1965.
- [29] J.A. McCleverty, Chem. Rev. 104 (2004) 403–418.
- [30] J.H. Enemark, R.D. Feltham, Coord. Chem. Rev. 13 (1974) 339–406.
- [31] I.-K. Choi, Y. Liu, D. Feng, K.-J. Paeng, M.D. Ryan, Inorg. Chem. 30 (1991) 1832–1839.
- [32] D. Lançon, K.M. Kadish, J. Am. Chem. Soc. 105 (1983) 5610–5617.
- [33] L.W. Olson, D. Schaeper, D. Lançon, K.M. Kadish, J. Am. Chem. Soc. 104 (1982) 2042–2044.
- [34] J. Pellegrino, S.E. Bari, D.E. Bikiel, F. Doctorovich, J. Am. Chem. Soc. 132 (2010) 989–995.
- [35] J. Pellegrino, R. Hübner, F. Doctorovich, W. Kaim, Chem. Eur. J. 17 (2011) 7868–7874.
- [36] N. Lehnert, V.K.K. Praneeth, F. Paulat, J. Comput. Chem. 27 (2006) 1338–1351.
- [37] D.P. Linder, K.R. Rodgers, Inorg. Chem. 44 (2005) 8259–8264.
- [38] C.E. Immoos, F. Sulc, P.J. Farmer, K. Czarnecki, D.F. Bocian, A. Levina, J.B. Aitken, R.S. Armstrong, P.A. Lay, J. Am. Chem. Soc. 127 (2005) 814–815.
- [39] F. Sulc, C.E. Immoos, D. Pervitsky, P.J. Farmer, J. Am. Chem. Soc. 126 (2004) 1096–1101.
- [40] R. Lin, P.J. Farmer, J. Am. Chem. Soc. 122 (2000) 2393–2394.
- [41] A.C. Montenegro, V.T. Amorebieta, L.D. Slep, D.F. Martín, F. Roncaroli, D.H. Murgida, S.E. Bari, J.A. Olabe, Angew. Chem. Int. Ed. 48 (2009) 4213–4216.
- [42] R.G. Serres, C.A. Grapperhaus, E. Bothe, E. Bill, T. Weyhermüller, F. Neese, K. Wieghardt, J. Am. Chem. Soc. 126 (2004) 5138–5153.
- [43] A.K. Patra, K.S. Dube, B.C. Sanders, G.C. Papaefthymiou, J. Conradie, A. Ghosh, T.C. Harrop, Chem. Sci. 3 (2012) 364–369.
- [44] S. Ye, J.C. Price, E.W. Barr, M.T. Green, J.M. Bollinger Jr., C. Krebs, F. Neese, J. Am. Chem. Soc. 132 (2010) 4739–4751.
- [45] M. Bayachou, R. Lin, W. Cho, P.J. Farmer, J. Am. Chem. Soc. 120 (1998) 9888–9893.
- [46] N.S. Gill, F.B. Taylor, Inorg. Synth. 9 (1967) 136–142.
- [47] W.R. Scheidt, M.E. Frisse, J. Am. Chem. Soc. 97 (1975) 17–21.
- [48] S.K. Sur, J. Magn. Reson. 82 (1989) 169–173.
- [49] G.R. Fulmer, A.J.M. Miller, N.H. Sherden, H.E. Gottlieb, A. Nudelman, B.M. Stoltz, J.E. Bercaw, K.I. Goldberg, Organometallics 29 (2010) 2176–2179.
- [50] F.A. Walker, M.-W. Lo, M.T. Ree, J. Am. Chem. Soc. 98 (1976) 5552–5560.
- [51] C.A. Reed, T. Mashiko, S.P. Bentley, M.E. Kastner, W.R. Scheidt, K. Spartaian, G. Lang, J. Am. Chem. Soc. 101 (1979) 2948–2958.
- [52] A.D. Boersma, H.M. Goff, Inorg. Chem. 21 (1982) 581–586.
- [53] SMART v5.626: Software for the CCD Detector System, Bruker AXS, Madison WI, 2000.
- [54] N. Walker, D. Stuart, Acta Crystallogr. A39 (1983) 158–166.
- [55] G.M. Sheldrick, SADABS, Area Detector Absorption Correction, University of Göttingen, Göttingen, Germany, 2001.
- [56] G.M. Sheldrick, SHELX-97, Program for Refinement of Crystal Structures, University of Göttingen, Göttingen, Germany, 1997.
- [57] G.M. Sheldrick, SHELXTL 6.1, Crystallographic Computing System, Siemens Analytical X-Ray Instruments, Madison, WI, 2000.
- [58] M.N. Burnett, C.K. Johnson, ORTEP-III, Report ORNL-6895, Oak Ridge National Laboratory, Oak Ridge, TN, 1996.
- [59] Z. Wei, M.D. Ryan, Inorg. Chem. 49 (2010) 6948–6954.
- [60] W.H. Harman, C.J. Chang, J. Am. Chem. Soc. 129 (2007) 15128–15129.
- [61] J.P. Bigi, W.H. Harman, B. Lassalle-Kaiser, D.M. Robles, T.A. Stich, J. Yano, R.D. Britt, C.J. Chang, J. Am. Chem. Soc. 134 (2012) 1536–1542.
- [62] N.A. Piro, M.F. Lichterman, W.H. Harman, C.J. Chang, J. Am. Chem. Soc. 133 (2011) 2108–2111.
- [63] A. Bondi, J. Phys. Chem. 68 (1964) 441–451.
- [64] A.W. Addison, T.N. Rao, J. Reedijk, J. van Rijn, G.C. Verschoor, J. Chem. Soc., Dalton Trans. (1984) 1349–1356.
- [65] L.E. Goodrich, F. Paulat, V.K.K. Praneeth, N. Lehnert, Inorg. Chem. 49 (2010) 6293–6316.
- [66] G.R.A. Wyllie, W.R. Scheidt, Chem. Rev. 102 (2002) 1067–1089.
- [67] G.R.A. Wyllie, C.E. Schulz, W.R. Scheidt, Inorg. Chem. 42 (2003) 5722–5734.
- [68] J. Conradie, A. Ghosh, Inorg. Chem. 50 (2011) 4223–4225.
- [69] V.K.K. Praneeth, C. Näther, G. Peters, N. Lehnert, Inorg. Chem. 45 (2006) 2795–2811.
- [70] K.M. Vogel, P.M. Kozlowski, M.Z. Zgierski, T.G. Spiro, J. Am. Chem. Soc. 121 (1999) 9915–9921.
- [71] N.G. Connelly, W.E. Geiger, Chem. Rev. 96 (1996) 877–910.
- [72] D.E. Bergbreiter, J.M. Killough, J. Am. Chem. Soc. 100 (1978) 2126–2134.
- [73] D. Savoia, C. Trombini, A. Umani-Ronchi, Pure Appl. Chem. 57 (1985) 1887–1896.
- [74] C.A. Kilner, M.A. Halcrow, Acta Crystallogr. C62 (2006) m437–m439.
- [75] D. Gwost, K.G. Caulton, Inorg. Chem. 12 (1973) 2095–2099.
- [76] S.E. Bari, M.A. Martí, V.T. Amorebieta, D.A. Estrin, F. Doctorovich, J. Am. Chem. Soc. 125 (2003) 15272–15273.
- [77] D.A. Bazylinski, T.C. Hollocher, J. Am. Chem. Soc. 107 (1985) 7982–7986.
- [78] M.A. Martí, S.E. Bari, D.A. Estrin, F. Doctorovich, J. Am. Chem. Soc. 127 (2005) 4680–4684.
- [79] S.A. Suárez, M.A. Martí, P.M. De Biase, D.A. Estrin, S.E. Bari, F. Doctorovich, Polyhedron 26 (2007) 4673–4679.
- [80] M. Hoshino, T. Baba, J. Am. Chem. Soc. 120 (1998) 6820–6821.
- [81] X.-Q. Zhu, J.-Y. Zhang, L.-R. Mei, J.-P. Cheng, Org. Lett. 8 (2006) 3065–3067.
- [82] C.-Y. Chiang, M.Y. Darenbourg, J. Biol. Inorg. Chem. 11 (2006) 359–370.
- [83] C.A. Reed, T. Mashiko, W.R. Scheidt, K. Spartaian, G. Lang, J. Am. Chem. Soc. 102 (1980) 2302–2306.
- [84] K.M. Kadish, R.K. Rhodes, Inorg. Chem. 22 (1983) 1090–1094.
- [85] K.N. Houk, B.N. Hietbrink, M.D. Bartberger, P.R. McCarren, B.Y. Choi, R.D. Voyksner, J.S. Stamler, E.J. Toone, J. Am. Chem. Soc. 125 (2003) 6972–6976.
- [86] L.L. Perissinotti, A.G. Turjanski, D.A. Estrin, F. Doctorovich, J. Am. Chem. Soc. 127 (2005) 486–487.